ACS Sustainable Chemistry & Engineering

pubs.acs.org/journal/ascecg

Research Article

# Duplex Process to Produce Ferromanganese and Direct Reduced Iron by Natural Gas

Jafar Safarian*

Cite This: *ACS Sustainable Chem. Eng.* 2021, 9, 5010−5026

Read Online

ACCESS | Metrics & More | Article Recommendations

**ABSTRACT:** The application of natural gas instead of solid carbon to produce ferromanganese is a way forward in sustainable development. Mass and energy balances for an integrated duplex process to produce ferromanganese and direct reduced iron (DRI) by natural gas were studied. The process consists of natural gas injection into molten ferromanganese yielding carbon and hydrogen in which the dissolved carbon into the molten metal bath reduces MnO from a coexisting molten slag that is produced from the smelting of manganese ore. Hydrogen and CO gases reduce solid manganese oxides and iron oxides in the Mn ore to MnO and Fe in the ferromanganese reactor burden. A hot gas with a significant amount of CO and $H_2$ leaves the reactor and is upgraded to a rich CO−$H_2$ gas mixture via methane use in a gas reformer. The obtained highly reducing gas is then used to reduce iron ore in a direct reduction reactor for DRI production, while the DRI reactor process gas is partly looped into the gas reformer and the rest is used in an energy recovery unit for electric power generation for the ferromanganese reactor. It is shown that the presented duplex process is more sustainable than the current commercial ferromanganese production process and its application is accompanied by about 50% less electric energy consumption and about 40% less $CO_2$ emission, excluding the source of electricity.

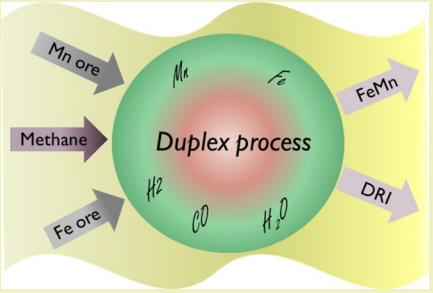


**KEYWORDS:** *ferromanganese, direct reduced iron, natural gas, sustainable, energy consumption, $CO_2$ emission*



## 1. INTRODUCTION

The theoretical basis for the main reactions in the ferromanganese process, and the idea of replacement of solid carbon with natural gas in a new process are described as follows.

**1.1. State of the Art.** The commercial production of ferromanganese is through the carbothermic smelting-reduction of manganese ores using submerged arc furnace (SAF) and blast furnace (BF) technologies.[1] The SAF technology is the dominant one nowadays regarding its several advantages compared to the BF. Metallurgical coke is the main solid carbon reductant that is used in SAF. The dependence of the process on the solid carbon use is in principle related to the thermochemistry of manganese monoxide (MnO) reduction, which is viable by carbon and not by $H_2$ and CO gases, as previously described.[2,3] In principle, the reduction of higher manganese oxides ($MnO_2$, $Mn_2O_3$, and $Mn_3O_4$) to MnO is possible by $H_2$[4] and CO gases.[5] Natural gas, which is rich in methane ($CH_4$), is a more sustainable alternative reductant for metal and ferromanganese production in comparison with metallurgical coke and, therefore, there has been a significant research interest in using this reductant.[2,3,6,7] However, the application of natural gas at elevated temperatures yields CO and $H_2$ gas mixtures and the reduction by these gases cannot proceed beyond MnO, and this has been the basis for many researchers to use natural gas for the prereduction of the ore as reviewed previously.[3] Regarding the fact that MnO can be reduced to metallic manganese through a carbothermic reduction via chemical reaction 1 and the produced CO gas is enough to reduce higher Mn oxides to MnO via chemical reactions 2−4, the application of a prereduction unit based on natural gas use to treat Mn ores is not advantageous from the reducing agent supply point of view. Obviously, the use of methane in a separate prereduction unit (directly or indirectly after reforming it to $H_2$ + CO) and then MnO reduction by solid carbon in a smelting step will increase the overall carbon use per unit mass of Mn produced. Strictly speaking, ideal situation is the maximum usage of CO that is generated via reaction 1 for reactions 2−4 without any more use of carbon (C from a methane source). In addition, the reduction reactions of manganese oxides by $H_2$ and CO gas mixtures (originating from methane) in which the less-exothermic reactions 5−7 than reactions 2−4 simultaneously taking place is not advantageous than the carbothermic route to benefit the process energy.

Received: November 19, 2020
Revised: February 24, 2021
Published: April 1, 2021

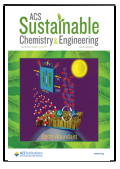

$$MnO + C(s) = Mn + CO(g)$$
$$\Delta H^{\circ}_{(25\,^{\circ}C)} = 274.3\ kJ/mol \quad (1)$$

$$2MnO_2 + CO(g) = Mn_2O_3 + CO_2(g)$$
$$\Delta H^{\circ}_{(25\,^{\circ}C)} = -203\ kJ/mol \quad (2)$$

$$3Mn_2O_3 + CO(g) = 2Mn_3O_4 + CO_2(g)$$
$$\Delta H^{\circ}_{(25\,^{\circ}C)} = -174\ kJ/mol \quad (3)$$

$$Mn_3O_4 + CO(g) = 3MnO + CO_2(g)$$
$$\Delta H^{\circ}_{(25\,^{\circ}C)} = -56\ kJ/mol \quad (4)$$

$$2MnO_2 + H_2(g) = Mn_2O_3 + H_2O(g)$$
$$\Delta H^{\circ}_{(25\,^{\circ}C)} = -163.7\ kJ/mol \quad (5)$$

$$3Mn_2O_3 + H_2(g) = 2Mn_3O_4 + H_2O(g)$$
$$\Delta H^{\circ}_{(25\,^{\circ}C)} = -135.1\ kJ/mol \quad (6)$$

$$Mn_3O_4 + H_2(g) = 3MnO + H_2O(g)$$
$$\Delta H^{\circ}_{(25\,^{\circ}C)} = -16.6\ kJ/mol \quad (7)$$

In ferromanganese production in SAF, solid carbon in the burden is in contact with $CO/CO_2$ gases and, therefore, the Boudouard reaction 8 occurs and causes both carbon material loss, electric energy loss, and more $CO_2$ emission per unit mass of the ferroalloy product than the ideal case of a Boudouard reaction-free process. As this reaction produces 2 mol CO per 1 mol consumed $CO_2$ and it is eventually oxidized to $CO_2$ through the SAF off-gas combustion by air, two times more $CO_2$ is generated than the consumed $CO_2$ by the Boudouard reaction. The Boudouard reaction in SAF causes more carbon use[8] and it consumes several hundred kW h electric energy per ton alloy produced, that is, 400 kW h for 475 kg coke use/ton ferroalloy.[9] Therefore, developing a technology to carry out the prereduction of the ore to MnO separately, and then the carbothermic reduction in a smelting furnace is beneficial and it has been claimed that 8.8, 13.5, and 20.4% electric energy is saved if the raw materials are preheated and reduced at 550, 650, and 950 °C, respectively.[10] Tangstad et al. calculated 22% electric energy saving by prereduction to 600 °C and showed that electric energy consumption depends also on the ore type and the oxygen level in the ore.[11] Obviously, the cost required to operate a separate prereduction unit may be more than that required to operate the SAF and it may be a main challenge for the process development.

$$C + CO_2(g) = 2CO(g) \qquad \Delta H^{\circ}_{(25\,^{\circ}C)} = 173.8\ kJ/mol \quad (8)$$

The carbothermic reduction of MnO in SAF occurs at elevated temperatures and mainly from a slag saturated of MnO, in the coke bed zone. The phase relations for the process and MnO reduction from the slag have been reported in the literature, and it has been experimentally indicated that the carbothermic reduction of MnO occurs by both solid carbon (coke particles) and the dissolved carbon in the high carbon ferromanganese (HCFeMn) bath.[12] It has been shown that the kinetics of MnO reduction by the dissolved carbon in Fe and Fe−Mn alloys is fast and Mn is transferred from the slag to the metal phase with a high rate.[13−17] The significant experimental studies about the MnO reduction from slags by solid carbon show activation energies in the range of 332−407 kJ/mol, while the reduction by the dissolved carbon in Fe−Mn melts occurs through a significantly lower activation energy in the range 90−197 kJ/mol.[18] Hence, the reduction of MnO from the ferromanganese slag can be done only by the dissolved carbon in the metal with no solid carbon material use, if proper slag/metal contact is maintained to attain a proper process rate.

**1.2. Direct Use of Methane: the Idea.** Regarding the presented points above, the application of natural gas to produce ferromanganese is feasible in an approach in which the carbon in methane is dissolved into the molten ferromanganese and it is simultaneously consumed for the MnO reduction from the molten slag. The released CO gas (due to MnO reduction) together with the $H_2$ from the methane cracking can then do the prereduction of Mn oxides to MnO. The methane cracking that yields the required dissolved carbon into the metal phase is via the following reaction.

$$CH_4(g) = \overline{C} + 2H_2(g) \qquad \Delta H^{\circ}_{(25\,^{\circ}C)} = 82.1\ kJ/mol \quad (9)$$

The dissociation of methane into C and $H_2$ is thermodynamically possible at temperatures higher than 548 °C, and methane cracking in a molten metal phase is consequently accompanied by C transfer (dissolution) into the melt, if there is solubility. The decomposition of methane has been widely reported in the literature mostly for hydrogen production using metallic catalysts and carbonaceous catalysts.[19] In some studies, the methane decomposition via its introduction into molten metal baths has been investigated after the Steinberg's studies.[20] Methane (and ethane) injection into the low melting point metal baths of lead and tin by Serban et al. indicated that the methane conversion is increased upon increasing the molten metal bath height and decreasing the gas flow rate at 750 °C.[21] They also showed that the methane conversion in the molten Sn is significantly increased with decreasing bubble size and bath temperature and they showed experimentally up to 70% methane conversion using their setup at 800 °C. The other studies about methane pyrolysis via bubbling into molten tin have shown moderate conversions under different applied experimental conditions.[22,23] Methane bubbling in a molten 27 mol % Ni−73 mol % Bi alloy column at 1065 °C by Upham et al. yielded 95% conversion.[24] These experimental studies have been on the metals that show low solubility of carbon (with the aim of hydrogen production and solid carbon separation). From the high-temperature thermodynamics point of view, however, it is expected to obtain better methane pyrolysis using metals that show high miscibility with carbon such as molten Fe−C and Mn−C alloys. A proof-of-concept test by the author, for this work, was done using a 20 mol % Fe−80 mol % Mn mixture in an alumina crucible in which methane was bubbled (melt height about 40 mm in a 35 mm inner crucible diameter) by 0.5 mm diameter bubbles with 0.1 normal liter per minute at 1500 °C in an induction furnace. During the experiment, a black smoke was observed over the melt, depicting some carbon black (soot) formation in the system. It was found by both mass balance and microstructural study (graphite precipitates in the alloy) that about 70% of the introduced carbon was dissolved into the molten ferromanganese alloy, and the rest was found as soot on the furnace walls. It is most likely possible that the methane conversion occurs completely; however, carbon is partly moved out from the melt due to a short residence time, or in other word


https://doi.org/10.1021/acssuschemeng.0c08462
ACS Sustainable Chem. Eng. 2021, 9, 5010−5026

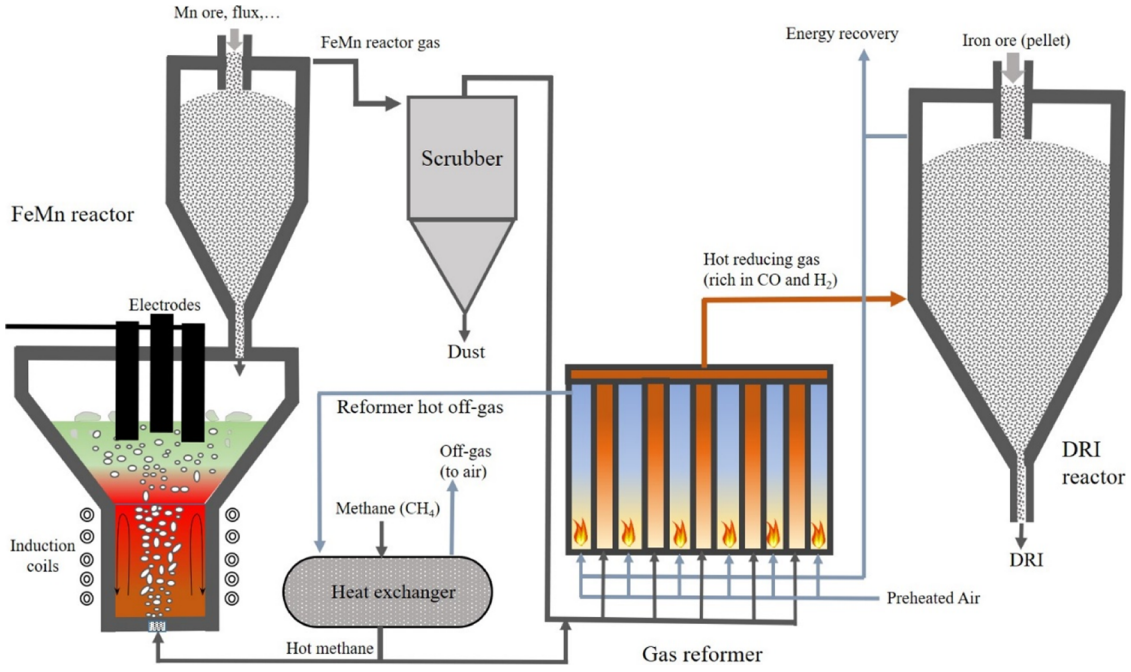


**Figure 1.** Schematic of the material flow for the main parts of the duplex FeMn-DRI process.

a small size of the reactor. In short, methane decomposition through injection into molten ferromanganese is viable.

This work presents an overview about an integrated process in which natural gas is used as a reducing agent to produce HCFeMn, and, in addition, a direct reduced iron (DRI) reactor. This technology does not exist entirely today, however, it can be developed in future regarding highly global interest in the development of low-carbon footprint processes and the fact that manganese ferroalloys are utilized in the steel industry. In this process, the carbon in methane supplies the required reducing agents for the ferromanganese reactor. Moreover, the ferromanganese reactor process gas contains high amounts of CO and $H_2$ gases and is further used to make a hot reducing gas for a DRI reactor. It is shown by mass and energy balances that this process, which is hereafter called "Duplex FeMn-DRI process", provides a sustainable integrated approach with significantly lower $CO_2$ emission and energy consumption than the stand-alone current technologies for ferromanganese and DRI production.

## 2. PROCESS OVERVIEW AND MATERIAL FLOW

Figure 1 shows schematically the material flow for the main parts of the duplex FeMn-DRI process in which two reactors for FeMn and DRI production are in continuous operation. Considering the current industrial situation in which the use of Mn ore in SAF is common and the use of iron ore pellet is more common for DRI production, these forms of the main raw materials for the two reactors are considered. In the DRI reactor, no other charge material is used; however, in the FeMn reactor, a flux is used to benefit the ore smelting and control the produced slag chemistry. Compared with the existing SAF furnaces, the FeMn reactor in the Duplex process has no solid carbon material in the charge, while methane is injected to the molten metal bath down in the reactor. The produced molten HCFeMn in the FeMn reactor and the corresponding slag are partially tapped in proper time intervals like the SAF process, or the well-known processes in the ferrous industry. However, some metals and slags are held in the reactor to maintain proper operation. The produced sponge iron in the DRI reactor is discharged continuously, and the production of both cold and hot DRI is possible, depending on the reactor design and the downstream steelmaking process. DRI production technologies are well known and a DRI reactor with a reformer unit as shown in Figure 1 is considered for the Duplex process.

An important issue to consider about the proposed process is the quality of the produced ferromanganese regarding the carbon content, as this type of ferroalloy is classified based on the carbon content as HCFeMn, medium-, and low-carbon ferromanganese products. In order to clarify this, the rate of methane decomposition and the simultaneous dissolved carbon consumption were compared. For the performed experiment for methane decomposition through its purging into the Fe−80 mol % Mn melt, an apparent rate constant of $1.2 \times 10^{-5}$ m/s was estimated. This is much larger than the rate constant for MnO reduction by solid carbon that was typically calculated to be $1.8 \times 10^{-7}$ m/s based on the previously obtain experimental data,[25] for an average 40% MnO concentration and a typical slag density of about 3 g/cm$^3$. The rate constants for MnO reduction by the dissolved carbon are a couple of times larger, depends on slag and metal chemistry,[26] and it is in the range $3 \times 10^{-7}$ to $1.5 \times 10^{-6}$ m/s. These may indicate that the rate of carbon dissolution into the melt (from methane) is significantly higher than its consumption for MnO reduction, yielding a molten metal with carbon close to saturation and HCFeMn production. In practice, however, the production of low-carbon ferromanganese may be possible via adjusting the rate of methane introduction, which is advantageous with regard to no further refining for the metal decarburization.

Natural gas (methane) is used directly in the FeMn reactor and indirectly in the DRI reactor after being reformed to a hot reducing gas. It is preheated and then injected into the FeMn reactor and consequently the FeMn process gas, which is mainly consisted of $H_2$, CO, $CO_2$, and $H_2O$ components with a high chemical value ($H_2$ and CO), is treated in the gas reformer. It is worth mentioning that there will be negligible unreacted


https://doi.org/10.1021/acssuschemeng.0c08462
ACS Sustainable Chem. Eng. 2021, 9, 5010−5026

Table 1. Chemical Composition of Comilog MMA Ore on a Dry Basis (wt %) Selected for This Work

| $MnO_2$ | MnO | $Fe_2O_3$ | $SiO_2$ | $Al_2O_3$ | MgO | CaO | BaO | $K_2O$ | P | $CO_2$ | $XH_2O$[a] |
|---|---|---|---|---|---|---|---|---|---|---|---|
| 76.3 | 3.2 | 3.9 | 4.0 | 5.5 | 0.3 | 0.2 | 0.2 | 0.7 | 0.1 | 0.1 | 5.4 |

[a]Structural water.

methane in the process gas as methane conversion is almost completed in the molten metal bath due to the very high rate of methane decomposition. The methane decomposition at elevated temperatures occurs rapidly and it is approximated with a typical rate constant of about 828 $s^{-1}$ at 1500 °C for homogeneous decomposition to other gaseous species such as $C_2H_6$, $C_2H_4$, $C_2H_2$,[27] and the decomposition to carbon black occurs rapidly within short times such as 0.002 s. For instance, the conversion of $C_2H_2$ to carbon black was calculated with a rate of $5 \times 10^{10}$ $s^{-1}$ at 1500 °C based on the provided kinetic data in the literature.[28] The exposure of methane with molten ferromanganese may also enhance the rate of methane conversion via the catalytic effect of the Mn and Fe elements. For the duplex process, even if there is a small amount of unreacted methane in the ferromanganese reactor process gas, it is not a problem as more methane is added into it to feed the gas reformer. The produced hot reducing gas by the reformer is utilized in the DRI reactor as the reducing and heating agent. The DRI reactor gas outlet has considerable amounts of $H_2$ and CO and it is partly used as the fuel in the gas reformer burners. Moreover, to make a more energy-efficient process, the rest of this gas is used for electric power generation. In addition, the hot off-gas of the reformer is utilized to preheat the natural gas used in the process units.

From the technical point of view, the gas injection into molten metals has been applied widely in both ferrous and nonferrous metallurgical industries and it is feasible. On the other hand, significant $H_2$ and CO gases are generated in the molten metal bath and at the metal−slag interface and these may be advantageous for the process. They make a lot of turbulence in the system that provides a better contact of the metal and slag and enhances the rate of the reactions, like MnO reduction by the dissolved carbon in metal, and this may improve the process rate. Moreover, the turbulence provides better heat transfer in the system and between the metal and slag phases, providing more homogeneous phases and a smooth operation. In addition, foamy slag formation may improve the process with less energy consumption (in the case of graphite electrode use) and less refractory wear.

## 3. RESULTS AND DISCUSSION: DUPLEX PROCESS THERMOCHEMISTRY, MASS, AND ENERGY BALANCES

The study of thermochemistry of the duplex FeMn/DRI process and the corresponding material and energy balance calculations were carried out as follows. To do proper mass and energy balances, fundamental data about manganese and iron ores reduction were used. Equilibrium calculations were carried out, when needed. The applied procedures of calculations are described in detail so that readers from various engineering disciplines with different backgrounds can follow the work and understand the thermochemistry of the duplex process. The Heat and Material balance module in HSC Chemistry software version 9 was used to carry out the main calculations. For each process step, the input data for the calculations were the amount and temperature of the components in the feed to the process step, and the amount of the products and their temperatures at the outlet. The software does mass and energy balance for the process, or defined process steps.

**3.1. FeMn Reactor.** To do mass and energy balances for the FeMn reactor, a typical commercial manganese ore was considered with the chemical characteristics given in Table 1, which is a high grade Mn ore (Comilog MMA).[1] The applied methodology here, however, can be in principle applied for using any type of charge materials and mixtures. The other material that must be considered was quick lime flux, and this material has usually above 97% CaO (mostly CaO with a small amount of $CaCO_3$) and the type of its impurities may vary but it does not significantly affect the following calculations, the flux for FeMn reactor was considered to be 100% CaO for simplicity.

For the calculations, the production of slag and metal products with known compositions and tapping temperatures was considered. Moreover, typical temperature for the process gas was selected, while the considered temperatures for inside of the reactor parts were outlined based on the process thermochemistry.

*3.1.1. Mass Balance for the FeMn Reactor.* Based on the production of HCFEMn and slag with known compositions, the reactor charge and required methane were determined. The energy balance was then done regarding the chemical and thermal characteristics of the reactor input and output, and the chemical reactions in the reactor at different defined parts.

*3.1.1.1. Charge Materials and the Products.* To make a proper mass balance for the FeMn reactor, the chemical composition of HCFeMn was assumed as 82% Mn−11.5% Fe−7.5% C, which is a standard chemical composition for this product.[29] In addition, the chemical composition of the produced slag from the above Mn ore was fixed by considering a fixed ternary basicity of (CaO + MgO)/$SiO_2$ as unity and producing a slag containing 20% MnO, which is a fair approximation with high Mn recovery. It is worth noting that FeMn slag may contain much higher MnO, that is, 30−40% MnO, if it is further utilized in a silicomanganese process as the Mn source. Assuming the complete reduction of iron oxides and partial reduction of the manganese oxides (some is left as MnO in the slag), the mass of produced slag can be calculated using mass balance as

$$m_{\text{slag}} = \frac{\left(\sum_{i \neq \text{MnO}, \text{Fe}_2\text{O}_3, \ldots} C_i^{\text{Mn ore}} \times \frac{m_{\text{Mn ore}}}{100}\right) + m_{\text{flux}}}{100 - C_{\text{MnO}}^{\text{slag}}} \times 100 \quad [\text{kg}] \tag{10}$$

where $m_j$ is the mass of material j such as manganese ore and $C_i^j$ is the concentration of component i in material j in weight percent. For instance, CaO in Mn ore is $C_{\text{CaO}}^{\text{Mn ore}}$, and $C_{\text{MnO}}^{\text{slag}}$ is the concentration of MnO in the produced slag. The required mass of lime flux can be determined based on the target ternary basicity (equal to unity) using the following expression

$$m_{\text{flux(CaO)}} = (C_{\text{SiO}_2}^{\text{Mn ore}} - C_{\text{CaO}}^{\text{Mn ore}} - C_{\text{MgO}}^{\text{Mn ore}}) \times \frac{m_{\text{Mn ore}}}{100} [\text{kg}] \tag{11}$$



https://doi.org/10.1021/acssuschemeng.0c08462
ACS Sustainable Chem. Eng. 2021, 9, 5010−5026

This equation is obtained assuming that the more stable oxides than MnO are not reduced in the FeMn reactor and all end up in the slag phase, while Fe is completely transferred to the metal (complete reduction) and Mn oxides are reduced to MnO with a further partial reduction to metallic Mn. Considering the selected ore, this mass balance shows that 181 kg slag is produced per ton (metric tons) Mn ore, and the slag has correspondingly a chemical composition of 20.6% CaO−22.2% $SiO_2$−30.5% $Al_2O_3$−20% MnO−1.7% MgO−3.8% $K_2O$−1.1% BaO−0.1% P (in mass percentage). As the amount of slag and its chemical composition are known for specific mass of the ore consumed, the amount of the produced metallic Mn can be calculated by mass balance for the Mn element. The quantity of the produced metal can be determined regarding the ore and product characteristics

$$m_{\mathrm{HCFeMn}} = \left[ (C_{\mathrm{Mn}}^{\mathrm{Mn\ ore}} \times m_{\mathrm{Mn\ ore}}) - C_{\mathrm{MnO}}^{\mathrm{slag}} \times m_{\mathrm{slag}} \times \frac{M_{\mathrm{Mn}}}{M_{\mathrm{MnO}}} \right] \times \frac{100}{C_{\mathrm{Mn}}^{\mathrm{FeMn}}} [\mathrm{kg}] \quad (12)$$

where $M_i$ denotes the molecular mass of component i. Equation 12 yielded about 592 kg HCFeMn per ton of the Mn ore consumed.

To produce the standard HCFeMn with 82% Mn−11.5% Fe−7.5% C composition, the addition of Fe and C is needed. Iron can be added through hematite ore use from the economic point of view, and considering a high-grade hematite ore (100% $Fe_2O_3$ here for simplicity) and its complete reduction in the FeMn reactor, the required amount of hematite can be calculated as

$$m_{\mathrm{hematite}} = \frac{M_{\mathrm{Fe_2O_3}}}{M_{\mathrm{Fe}}} \left[ \left( C_{\mathrm{Mn}}^{\mathrm{Mn\ ore}} \times \frac{m_{\mathrm{ore}}}{100} - C_{\mathrm{MnO}}^{\mathrm{slag}} \times \frac{M_{\mathrm{Mn}}}{M_{\mathrm{MnO}}} \right) \times \frac{C_{\mathrm{Fe}}^{\mathrm{FeMn}}}{C_{\mathrm{Mn}}^{\mathrm{FeMn}}} \right] - \frac{C_{\mathrm{Fe_2O_3}}^{\mathrm{Mn\ ore}}}{100} \times m_{\mathrm{Mn\ ore}} [\mathrm{kg}] \quad (13)$$

This equation showed that the addition of 58 kg hematite is required to produce a HCFeMn containing 11.5% Fe, when 1 ton of the above Mn ore is used.

*3.1.1.2. Required Methane.* The carbon for the FeMn reactor is supplied by the methane cracking and it goes into the HCFeMn product (7.5 wt % C) and the rest is consumed for MnO reduction from the slag phase, at the slag−metal interface. As discussed above, the rate of methane cracking is much higher than C consumption for MnO reduction and so the MnO reduction may control the process rate and consequently the rate of methane introduction. It is emphasized here that MnO reduction is taking place only by the dissolved carbon in the liquid metal. Hence, considering the chemical reaction 1, the total required carbon can be determined as

$$m_{\mathrm{carbon}} = \frac{M_{\mathrm{C}}}{M_{\mathrm{MnO}}} \left[ \left( C_{\mathrm{Mn}}^{\mathrm{Mn\ ore}} \times \frac{m_{\mathrm{Mn\ ore}}}{100} \times \frac{M_{\mathrm{MnO}}}{M_{\mathrm{Mn}}} \right) - m_{\mathrm{MnO}}^{\mathrm{slag}} \right] + C_{\mathrm{c}}^{\mathrm{FeMn}} \times m_{\mathrm{FeMn}} [\mathrm{kg}] \quad (14)$$

The first term on the right of eq 14 is the carbon use for MnO reduction, and the second term is the remained carbon in saturation in HCFeMn. Obviously, the required corresponding mass of methane is

$$m_{\mathrm{methane}} = \frac{M_{\mathrm{CH_4}}}{M_{\mathrm{C}}} \times m_{\mathrm{carbon}} [\mathrm{kg}] \quad (15)$$

This mass balance provided the need of the consumption of about 207 kg of methane per ton of ore. Around 28.6% of the carbon from the methane cracking goes to the metal product, and the remaining 71.4% contributes in the reduction of MnO from the slag.

*3.1.1.3. Burden Zone Reactions and the Process Gas.* Considering the masses of the carbon that react with MnO in the slag and hydrogen formed from methane cracking, the number of moles of CO and $H_2$ gas that leave the molten slag−metal bath can be determined as

$$n_{\mathrm{CO}} = \frac{1}{M_{\mathrm{CO}}} \left[ \left( C_{\mathrm{Mn}}^{\mathrm{Mn\ ore}} \times \frac{m_{\mathrm{ore}}}{100} \times \frac{M_{\mathrm{MnO}}}{M_{\mathrm{Mn}}} \right) - m_{\mathrm{MnO}}^{\mathrm{slag}} \right] [\mathrm{kmol}] \quad (16)$$

$$n_{\mathrm{H_2}} = \frac{2}{M_{\mathrm{CH_4}}} m_{\mathrm{methane}} [\mathrm{kmol}] \quad (17)$$

For the considered ore here, a gas composition of 73.7% $H_2$ and 26.3% CO, which is for about 35 kmol gas mixture per ton ore, was calculated. This highly reducing hot gas mixture will then interact with the solid charge in the burden and the chemical reactions 2−7 will take place, and in addition the following reactions occur for $Fe_2O_3$ reduction

$$3Fe_2O_3 + CO(g) = 2Fe_3O_4 + CO_2(g) \quad \Delta H_{(25\ ^\circ C)}^{\circ} = -35.4\ \mathrm{kJ/mol} \quad (18)$$

$$Fe_3O_4 + CO(g) = 3FeO + CO_2(g) \quad \Delta H_{(25\ ^\circ C)}^{\circ} = 16.15\ \mathrm{kJ/mol} \quad (19)$$

$$FeO + CO(g) = Fe + CO_2(g) \quad \Delta H_{(25\ ^\circ C)}^{\circ} = -10.84\ \mathrm{kJ/mol} \quad (20)$$

$$3Fe_2O_3 + H_2(g) = 2Fe_3O_4 + H_2O(g) \quad \Delta H_{(25\ ^\circ C)}^{\circ} = 5.77\ \mathrm{kJ/mol} \quad (21)$$

$$Fe_3O_4 + H_2(g) = 3FeO + H_2O(g) \quad \Delta H_{(25\ ^\circ C)}^{\circ} = 57.3\ \mathrm{kJ/mol} \quad (22)$$

$$FeO + H_2(g) = Fe + H_2O(g) \quad \Delta H_{(25\ ^\circ C)}^{\circ} = 30.3\ \mathrm{kJ/mol} \quad (23)$$

The prereduced charge that contains MnO and metallic iron is further smelted in the hot zone of the reactor. It must be emphasized here that the high amount of the produced $H_2$−CO gas mixture is enough and much more than the required gas to reduce all the Mn and Fe oxides in the charge to MnO and Fe species. As the $H_2$ content of the gas phase in the high-temperature region is much higher than the CO content, the direct reduction reactions are mainly via hydrogen gas. In particular, the reduction by $H_2$ is preferable at elevated temperatures than by the CO gas, as the CO gas is very stable compared to the $CO_2$ gas (the product of the CO gas consumed for reduction) at high temperatures such as 1000 °C. Regarding a temperature profile in the reactor burden, the gas components


https://doi.org/10.1021/acssuschemeng.0c08462
ACS Sustainable Chem. Eng. 2021, 9, 5010−5026

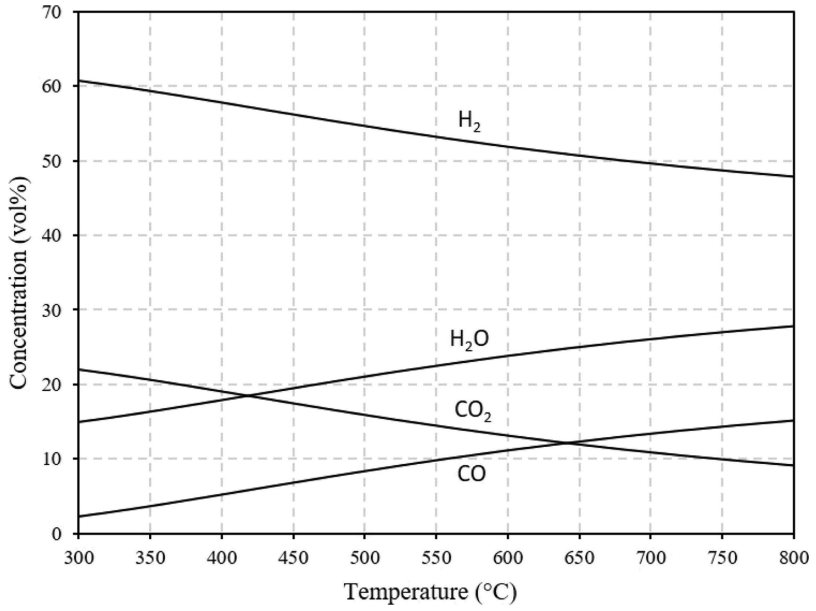


**Figure 2.** Equilibrium composition of the FeMn reactor process gas at different temperatures calculated by HSC Chemistry.

react with each other in addition to reacting with the solid charge particles, and thus the composition of the FeMn reactor gas outlet can be assumed close to equilibrium, which can be estimated considering the water gas shift reaction

$$CO(g) + H_2O(g) = CO_2(g) + H_2(g)$$
$$\Delta H^{\circ}_{(25\,^{\circ}C)} = -41.1\ \text{kJ} \quad (24)$$

The water gas shift reaction is an exothermic reaction that is more favorable at lower temperatures. Considering the amount of CO, $CO_2$, $H_2$, and $H_2O$ gases after the reduction of the ore and including the structural $H_2O$ and $CO_2$ in the Mn ore, the equilibrium composition of the gas phase at different temperatures was calculated as shown in Figure 2. For instance, if the FeMn reactor process gas temperature is 400 °C, the composition of the gas is approximately 57.4% $H_2$, 5.6% CO, 18.3% $H_2O$, and 18.7% $CO_2$ and totally about 38.1 kmol gas is produced per one ton ore.

Regarding the above results, the overall FeMn reactor mass balance is shown in Figure 3 for one ton of the HCFeMn

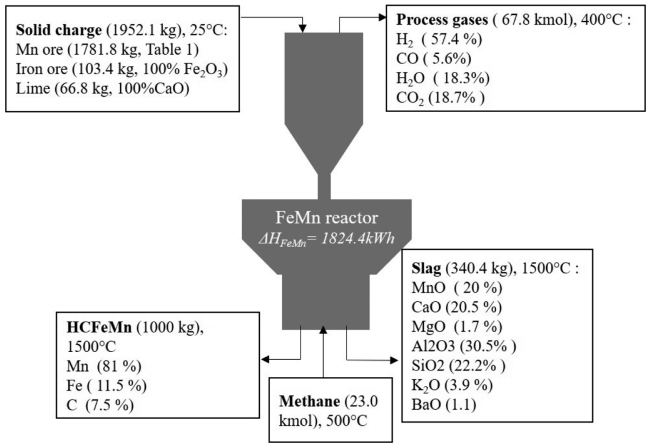


**Figure 3.** Overall mass balance for the FeMn reactor and the characteristics of its inputs and outputs.

product. As seen, the mass of the tapped metal is about half of that of the solid charge and is three times higher than that of the slag. The reactor has a significant amount of process gas (with about 64% reducing components of $H_2$ and CO) and it is around three times higher than the injected methane. This gas volume increase is due to the formation of 1 mol carbon and 2 mol hydrogen through the chemical reaction 9 and further conversion of most of this carbon to the CO gas. A portion of $H_2$ and CO gases are converted to $H_2O$ and $CO_2$ components with the same number of moles due to the reduction chemical reactions presented above. The small higher volume of the process gas (67.8 kmol) than the stoichiometric volume that was obtained for the reduction reactions (67.3 kmol/t ore) is due to the dissociation of hydrates and calcite components of the solid charge.

*3.1.2. Energy Balance for the FeMn Reactor.* To study the required energy for the operation of the FeMn reactor, its energy balance was done by calculating the enthalpy changes regarding the main chemical reactions and the above mass balance results. It was assumed that the solid materials are charged at room temperature, the process gas has 400 °C, the metal is tapped at 1500 °C, and a preheated methane to 500 °C is injected to the reactor (Figure 3). As the chemical reactions in the reactor are important, the energy balance was done by dividing the reactor into two zones; a *burden zone* that contains the solid charge materials and gases and a *melting zone* that contains both the molten slag and metal phases and gases.

*3.1.2.1. Burden Zone.* The interaction of the solid charge materials with the hot $H_2$ and CO gas mixture, i.e., generated in the melting zone was modeled via outlining the process chemistry, calculating the corresponding enthalpy changes, and equilibrium calculations.

*Heating and Reduction of Mn and Fe Oxides.* As mentioned above, all Mn oxides in the ore are reduced to MnO in the burden in contact with the hot reducing gas, and they are simultaneously heated to high temperatures, that is, to 1200 °C. Like the SAF process, MnO is in the solid form in the burden as the MnO content is high and any slag-type phase is almost saturated of MnO.[30,31] It is worth mentioning that depending on the type of the ores, different phases may be formed in the ore in


https://doi.org/10.1021/acssuschemeng.0c08462
ACS Sustainable Chem. Eng. 2021, 9, 5010−5026

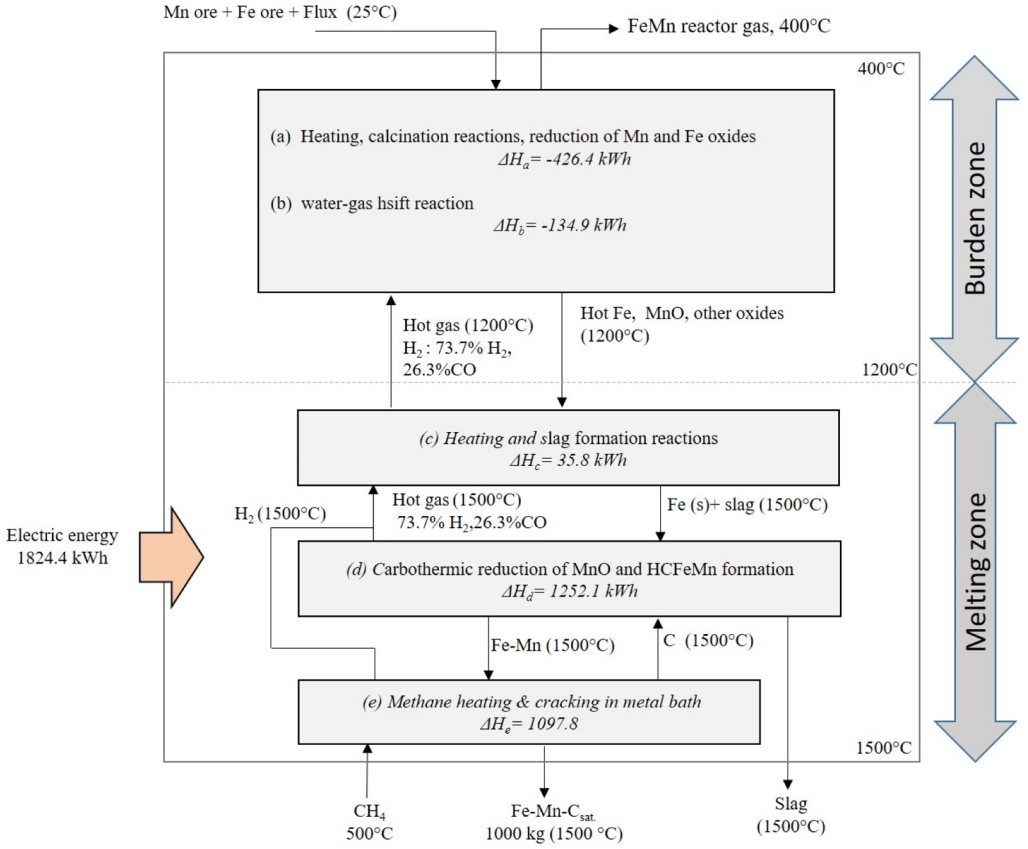


**Figure 4.** Energy balance model for the different zones of the FeMn reactor, based on the main reactions, phase changes, and defined temperatures.

the burden zone and some of them get partially or completely melted as studied by Sorensen et al.[32] Their equilibrium calculations by FactSage showed that liquid slag phases are formed in Groote Eylandt ore fine particles calcined and reduced by $H_2$ at 800−1200 °C, but not for Wessels ore treated under the same conditions. Their similar calculations indicated liquid slag formation possibility in Gabonese ore particles calcined and reduced by CO at 800−1200 °C, but not for CVRD ore (a well-known Mn ore) treated under the same conditions. Their X-ray diffraction quantitative analysis of the reduced Gabonese ore, however, indicated that it has different phases compared to those identified using FactSage calculations, and the main phases (manganosite and tephorite) were the same as those of the CVRD-reduced sample. The difference between their obtained experimental results compared to their equilibrium calculations may be due to kinetic issues (solid-state diffusion requirements). Hence, the smelting of the lump ore components and flux particles may not significantly occur up to 1200 °C as the dominant phases such as MnO, $Ca_2SiO_4$, $Mn_2SiO_4$, and metallic Fe have higher melting temperatures than minor coexisting molten or semimolten phases in the slag. Therefore, a typical highest temperature for the burden as 1200 °C is fairly acceptable; however, in practice it can be adjusted to lower temperatures regarding the type of the ore, and considering this temperature for the calculations here does not affect the overall heat balance calculations. Cheraghi et al.[33] indicated that the reduction of the size of the ore will increase the formation of slag type phases during calcination and reduction via providing a significantly higher contact area between the ore components. Hence, if the agglomerates of manganese ore fines/concentrates are used as the reactor feed, more slag type phases may be formed compared with lump ore, and it may cause the particle fusion and clustering (not smelting). Currently, there are technical solutions to minimize the clustering such as coating the agglomerates by lime, cement, and so forth or using declustering units such as the common one in the Miderx reactors. Simultaneous to Mn oxide reduction, $Fe_2O_3$ in the charge is reduced to metallic iron. The reduction of these oxides occurs by both $H_2$ and CO gases, however, as the water gas shift reaction in the system was considered, it does not matter that which reductant is interacting with the oxides. Hence, considering the conversion of 1 mol $H_2$ to $H_2O$ in 1 mol of $MnO_2$ to MnO, the $H_2$ consumption and the corresponding $H_2O$ production were calculated. Moreover, it was assumed that $Fe_2O_3$ reduction to Fe occurs by $H_2$ gas, 3 mol of $H_2$ gas is consumed per 2 mol $Fe_2O_3$, giving 4 mol Fe and 3 mol $H_2O$ gas. These assumptions provided information to do heat balance calculations for the heating and chemical reactions in the burden zone, excluding the water gas shift reaction. It is worth mentioning that some amount of $H_2O$ gas from the charge moisture, and $CO_2$ gas from the calcite is added into the gas phase. Consequently, the heat balance calculations yielded a heat balance of about—426 kWh/t HCFeMn for this main part of the burden zone as shown in Figure 4, where the solid charge is converted to hot particles/agglomerates (part (a)). This negative number is related to both the high enthalpy of the hot reducing gas and the significant exothermic reactions in the burden due to the main chemical reactions 2−7. Obviously, some heat is used for the reduction of $Fe_2O_3$ (about 15 kW h/kg FeMn), calcination of calcite, and heating of the solid charge from room temperature to 1200 °C.

*Water Gas Shift Reaction.* The enthalpy change due to the water gas shift reaction was calculated assuming it occurs at 400



https://doi.org/10.1021/acssuschemeng.0c08462
ACS Sustainable Chem. Eng. 2021, 9, 5010−5026

°C and the FeMn reactor gas is leaving the reactor at the same temperature. As the reaction is exothermic, it releases heat and there is around −134.9 kW h heat is generated due to this reaction.

Considering the a and b parts above, there is a net heat generation in the burden zone of about −561 kW h/t HCFeMn due to the exothermic reactions and the hot gas that is introduced to this zone. In the model here, the highest temperature for the gas and solid charge was considered as 1200 °C, and the amount of heat generated may be different if another temperature is considered. In order to evaluate this effect, the heat balance calculations were run for different temperatures and it was found that the net heat generation is −521, −542, −581, and −602 kW h/t HCFeMn for the selected highest zone temperatures of 1000, 1100, 1300, and 1400 °C, respectively. It is worth mentioning that the calculations for 1300 and 1400 °C are only for comparison and they are inappropriate for the burden zone, according to the above discussions. Obviously, the selection of the highest temperature for the defined burden zone (between 1000 and 1200 °C) has a small effect on the total enthalpy change. A part of the generated heat in the burden zone is partially transported into the melting zone by the hot materials and heat transport mechanisms, and some is lost from the reactor body as any other high temperature reactor, or it may cause higher temperature for the process gas.

*3.1.2.2. Melting Zone.* The hot solid calcined and prereduced charge is smelted, and the molten slag and metal phases are produced in the melting zone via the heat supply by electricity. In the model, it was assumed that all the hot materials are more heated by the hot gas to 1500 °C and then smelting reactions occur at 1500 °C. This step is then followed by a carbothermic reduction and simultaneous methane cracking steps as illustrated in Figure 4. Energy balances for these process parts were done as follows.

*Slag Formation Reactions.* In the slag formation step, the prereduced charge is heated from 1200 °C to about 1500 °C by the hot gas stream, while the gas is cooled down to 1200 °C before entering the burden zone. Considering the mass balances and compositions of the phases, the enthalpy change was calculated about—113 kW h/t HCFeMn for only heating the charge. However, in this zone, slag-forming reactions occur and the related enthalpy changes must be estimated. To approximate these enthalpy changes, the formation of the slag that is consisted of all oxides except MnO can be considered and then the enthalpy changes due to the melting and dissolution of MnO into the slag be added. In this case, the energy required for the formation of a $CaO–Al_2O_3–SiO_2$ slag, containing 28.1 wt % CaO, 41.6 wt % $Al_2O_3$, and 30.3 wt % $SiO_2$ (considering the mass and composition of the slag described in Section 3.1) per ton metal product, was determined to be about −25 kW h. This value was calculated assuming that the slag is initially formed through the formation of $CaO·SiO_2$ and $CaO·Al_2O_3·SiO_2$ molten components and their further mixing with a negligible enthalpy change due to mixing. Moreover, it was a fair approximation to consider negligible enthalpy changes due to the dissolution of the minor components of the charge (MgO, BaO, and $K_2O$) into this slag.

According to the literature, MnO in the charge of SAF is dissolved from a solid form into a slag saturated of MnO and further MnO reduction from the slag occurs, depending on the process conditions.[30] To calculate the heat required for MnO smelting at the process temperature (1500 °C), the sum of the enthalpy changes for heating the solid MnO from 1500 to 1882 °C (MnO melting point), the enthalpy changes due to the fusion of MnO at 1882 °C, and the enthalpy changes due to cooling the liquid MnO from 1882 to 1500 °C were calculated. This provided an enthalpy change of 191.5 kW h/t FeMn product. This MnO is then dissolved in a slag containing 20 wt % MnO (assumed above). The activity of MnO in this slag was calculated based on the slag chemistry according to the literature[34]

$$\ln a_{MnO} = \ln\left(\frac{X_{MnO}}{X_{MnO_{sat}}}\right) - 5.3\left(1 - \frac{X_{MnO}}{X_{MnO_{sat}}}\right)^2 \quad (25)$$

where $X_{MnO}$ and $X_{MnO_{sat}}$ are the molar fractions of MnO in the slag and that at saturation, respectively. The latter parameter for the process slag (20% MnO−22.2% $SiO_2$−30.5% $Al_2O_3$−20.5% CaO−1.7% MgO) was estimated to be $X_{MnO_{sat}}$ = 0.49 using FactSage thermodynamic software, which corresponds to 35 wt % MnO. Hence, the activity of MnO in the slag was obtained to be $a_{MnO}$ = 0.21 (standard state is liquid pure MnO), and correspondingly an activity coefficient of $\gamma_{MnO}$ = 0.77 was obtained. Assuming a regular solution model here, the changes in the partial molar enthalpy of mixing of MnO in solutions were calculated and this yielded an enthalpy change of about −18 kW h/t HCFeMn. Consequently, the total energy consumption for the melting and dissolution of MnO into the slag was obtained to be around 174 kW h/t HCFeMn. Hence, the total heat consumption for the slag-making reactions and continuous dissolution of MnO into the slag was estimated to be about 36 kW h/t HCFeMn as given in Figure 4.

*Carbothermic MnO Reduction and HCFeMn Formation.* The required energy for the carbothermic reduction of MnO by the dissolved carbon in molten ferromanganese can be calculated regarding the enthalpy change of the chemical reaction 1 and considering the reduced mass of MnO in the process that was determined by mass balance above for liquid Mn formation. These calculations yielded 0.08 kW h/mol MnO at 1500 °C, and the consumption of about 1247 kW h/t HCFeMn product.

The energy required for the formation of the molten alloy is not significant and it was estimated considering the latent heat of fusion of produced metallic iron (in the burden zone) and then the enthalpy change due to mixing with the molten Mn. The energy required for the melting of iron was calculated to be about 8 kW h/t HCFeMn. The change of the enthalpy of mixing of Fe and Mn was estimated to be about −2.5 kW h/t HCFeMn considering the small enthalpy of mixing for the Fe−Mn alloys.[35] Neglecting the enthalpy changes due to carbon dissolution, the overall heat change in the formation of liquid alloy is hence about 5 kW h/t HCFeMn.

Considering the above results, the energy balance for the model unit (d) for both the carbothermic reduction of MnO and alloy formation was estimated to be 1252 kW h/t HCFeMn. Compared to the former model units (a) to (c), it is obvious that the carbothermic reduction of MnO is the most energy-consuming reaction and although this energy in the reactor is partially compensated from the available thermal and chemical energy in the reactor, the required heat must be mostly supplied by electric power as schematically shown in Figure 1. It must be noted here that such an amount of heat is currently supplied by graphite electrodes in commercial SAF and is technologically feasible.

*Heating and Cracking of Methane.* The cracking of methane, reaction 9, to dissolved C and $H_2$ gases is an



https://doi.org/10.1021/acssuschemeng.0c08462
ACS Sustainable Chem. Eng. 2021, 9, 5010−5026

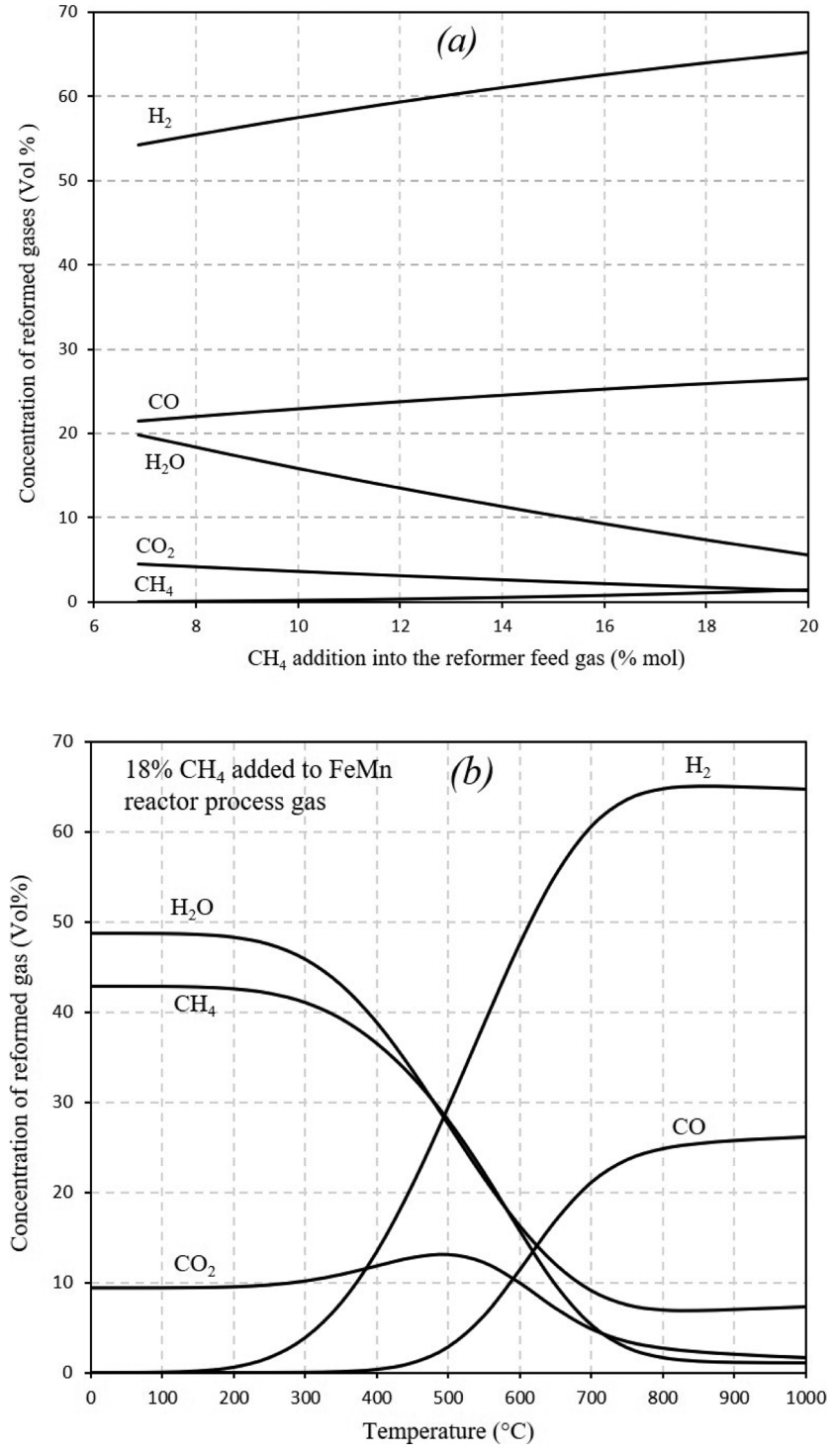


**Figure 5.** (a) Effect of methane addition on the composition of the reformed gas and (b) effect of reforming temperature on the composition of the reformed gas, considering 95% methane conversion.

endothermic reaction. The required energy to heat (from 500 °C) and crack methane can be calculated considering the consumed methane volume and its conversion to C and $H_2$ gases at 1500 °C. The calculation gave an energy consumption of 1098 kW h/t HCFeMn as shown for the unit module (e) in Figure 4, assuming no heat loss from the reactor body. It is worth mentioning that as the temperature for the reaction 9 is high (1500 °C) and there is a huge amount of Mn and Fe in contact with methane, methane is rapidly cracked to C and $H_2$ components with no kinetic barrier, and it was assumed that the methane conversion is complete, according to the above discussions. Compared to the other reaction unit models, it is seen that significant energy is required for methane cracking as it is endothermic.

*3.1.3. Overall Mass and Energy Balance of the FeMn Reactor.* The input and output masses for the whole FeMn reactor (Figure 4) show that the amount of slag that is produced per unit mass of metal product is relatively lower than the industrial situation for SAF. This is due to the considered low MnO concentration in the slag product (about 20%) compared



https://doi.org/10.1021/acssuschemeng.0c08462
ACS Sustainable Chem. Eng. 2021, 9, 5010−5026

to the processes in which the slag is further used for silicomanganese production.[1,36] It is worth mentioning that there are currently SAF units in operation with about 20% MnO in the tapped slag.[9] On the other hand, in the SAF process, the ash components of the solid carbon materials end up in the slag. Moreover, in this study, a high Mn ore grade is considered and in many industrial situations, lower Mn ore grades are utilized, yielding higher amounts of slag.

The required electric energy for the FeMn reactor was calculated as the sum of the above energy balances for unit models (a) to (e), which is about 1824 kW h/t HCFeMn. This energy can be supplied by graphite electrodes or induction to the hot metal bath, or a combination of both as schematically shown in Figure 1. Depending on the size and geometry of the reactor, the use of electrodes and induction may vary, and it is more related to furnace design.

**3.2. Gas Reformer Unit.** The FeMn reactor hot process gas has a significant amount of $H_2$ and CO gases (more than 60%) and the most sustainable approach is its utilization rather than its burning with air. As the proposed duplex process here intends to use it for DRI production, we consider its treatment in a gas reformer to attain a reducing gas for the DRI reactor. Hence, mass and energy balance calculations for the gas reformer are carried out as follows.

For a DRI unit, a proper gas composition can be a gas containing around 90% of the $H_2$ + CO gas mixture or a higher reducing potential. For instance, a typical feed-reducing gas for a Midrex reactor is 55% $H_2$, 35% CO, 6% $H_2O$, 2% $CO_2$, and 1% $N_2$, if we consider the Midrex NG process.[37] The FeMn reactor process gas contains some $CO_2$ and $H_2O$ and these gases can be converted to CO and $H_2$ gases upon exposure to $CH_4$ in the gas reformer (Figure 1). Although many reactions occur in the reformer tubes, the following main reactions can illustrate the gas reforming at elevated temperatures

$$CH_4(g) + H_2O(g) = CO(g) + 3H_2(g)$$
$$\Delta H^{\circ}_{1000\,^{\circ}C} = 225.9\ \text{kJ/mol} \quad (26)$$

$$CH_4(g) + CO_2(g) = 2CO(g) + 2H_2(g)$$
$$\Delta H^{\circ}_{1000\,^{\circ}C} = 258.1\ \text{kJ/mol} \quad (27)$$

To calculate the required $CH_4$ to produce a reducing gas at a typical temperature of 1000 °C, a couple of equilibrium calculations were carried out by HSC Chemistry and the results are shown in Figure 5. As seen, the introduction of about 18 vol % of $CH_4$ (15 kmol $CH_4$) into the FeMn reactor hot process gas yields a gas mixture with an approximate composition of 64.1% $H_2$, 25.9% CO, 7.2% $H_2O$, 1.7% $CO_2$, and 1.0% $CH_4$ at 1000 °C, assuming 95% conversion of methane. This conversion is a fair approximation as in reality the complete conversion of methane does not occur (equilibrium concentration is calculated to be 0.01% $CH_4$) due to a relatively short residence time of the gas in the reformer tubes. Figure 5a reveals that more than 18% $CH_4$ addition into the FeMn reactor process gas yields a hot reducing gas with more than 90% $H_2$ and CO gases, and hence it is proper to fix this amount of methane usage. On the other hand, the equilibrium calculations at different temperatures for this methane addition (Figure 5b) show that the reformer process gas composition is not significantly changed at temperatures above 800 °C, indicating that the assumed process temperature for the reformer is appropriate.

The energy balance for the gas reforming, which occurs in the reformer tubes, is shown in Figure 6. As seen, if preheated

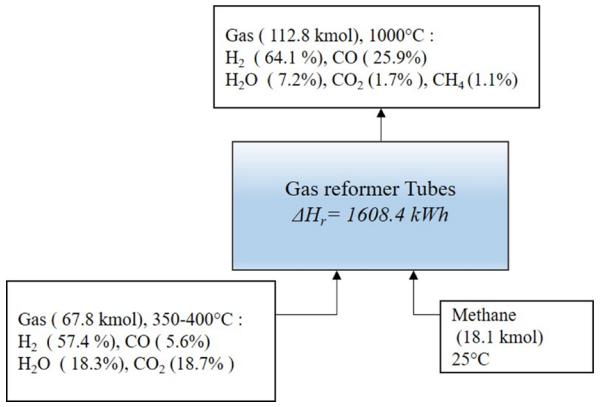


**Figure 6.** Overall mass balance and the characteristics of the input and output for the reformer tubes, considering 18% methane addition to the FeMn reactor process gas and 95% conversion of methane.

methane to 500 °C is used, about 1608 kW h/t HCFeMn heat is needed for both the heating of the gases to the reaction temperature and supplying the heat for the endothermic reactions 26 and 27. This required heat is completely supplied by burning a portion of the DRI reactor process gas by air, which is described later in Section 4.

In practice, the temperature of the FeMn reactor process gas is decreased in the scrubber (Figure 1), and its magnitude is dependent on the gas composition and the characteristics of the gas-cleaning unit. The enthalpy of the ferromanganese process gas (about 68 kmol) was calculated to be about −789, −791, and −795 kW h at 400, 375, and 350 °C, respectively. Hence, some thermal energy loss of the gas in the cleaning step does not affect the enthalpy of the gas as it is more in the form of chemical energies in the gaseous species. Therefore, assuming a typical temperature in the range of 350−400 °C (Figure 6) does not affect the above energy balance calculations for the reformer unit.

**3.3. DRI Reactor.** Any type of direct reduction furnaces to produce DRI can be installed adjacent to the FeMn reactor to utilize the hot reducing gas produced by the gas reformer. As an example, we consider a shaft furnace in this study as schematically shown in Figure 1. There are currently different technologies for the shaft furnaces such as Midrex, HYL, and so forth.[38] In the shaft furnace, the reducing gas is fed into the reactor and is in contact with the solid charge when it is moving upwards, while the iron ore particles/pellets in the burden are moving downwards continuously. This causes proper mass and heat exchange between the reactor burden and the process gas and, therefore, the iron oxides in the charge are reduced. The produced DRI can be cooled down in the lower part of the reactor like the traditional Midrex reactors, or it can be discharged as hot DRI or it can be briquetted to produce hot briquetted-DRI. In this study, the down part of the reactor is not included as it is more technology dependent and is of less importance regarding the process mass and energy balance.

*3.3.1. Mass Balance for the DRI Reactor.* In principle, the solid−gas reactions such as iron ore reduction are kinetic dependent in which different iron oxides and metallic iron phases coexist in the solid particles, according to the unreacted shrinking core model.[39] Therefore, the process simulation relies on the numerical solution of kinetic equations, which are


https://doi.org/10.1021/acssuschemeng.0c08462
ACS Sustainable Chem. Eng. 2021, 9, 5010−5026

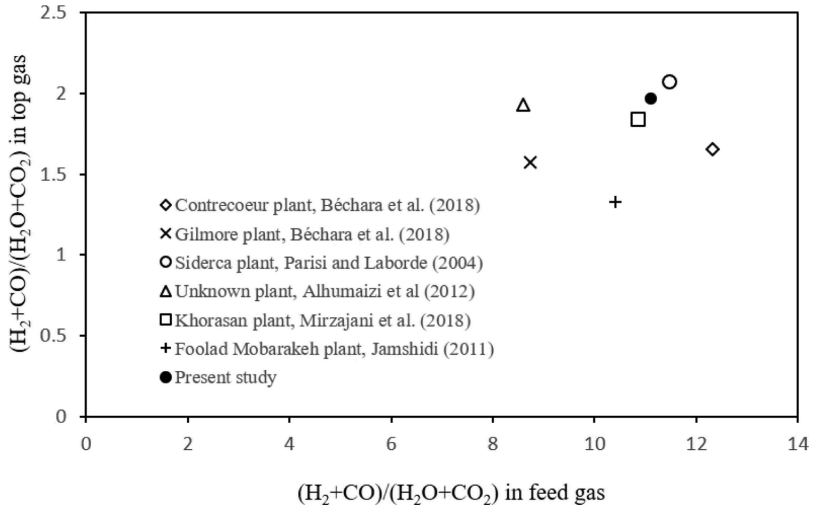


**Figure 7.** Molar ratio of $\frac{H_2 + CO}{H_2O + CO_2}$ in the feed gas and the top gas of industrial DRI reactors, and the obtained ratio for this study.

**Table 2. Chemical Characteristics of the Iron Ore Pellet and the Corresponding Produced DRI (wt %)**

| material | $Fe_2O_3$ | FeO | Fe−metal | $SiO_2$ | $Al_2O_3$ | MgO | CaO | $MnO_2$ | $TiO_2$ | P | S |
|---|---|---|---|---|---|---|---|---|---|---|---|
| oxide pellet | 95.80 | 0.14 | | 1.59 | 0.34 | 0.87 | 0.75 | 0.03 | 0.1 | 0.052 | 0.004 |
| DRI | | 6.97 | 87.75 | 2.2 | 0.47 | 1.2 | 1.04 | 0.04[a] | 0.14 | 0.07 | 0.01 |

[a]MnO.

connected also to the thermodynamic equilibrium for the chemical reactions 18−23, and the water gas shift reaction 24. The simulations of industrial DRI reactors carried out using different approaches have been reported in the literature and it is possible to simulate the whole reactor.[40−44] As the simulation of the reactor is not the aim of this work, fair approximations were done to fix the characteristics of the outlet top process gas close to the industrial reactors. Figure 7 compares the relationship between the molar ratio of $\frac{H_2 + CO}{H_2O + CO_2}$ in the feed gas and the top gas of industrial DRI reactors (Midrex modules) found in the literature. This figure shows that this ratio in the feed gas is between 8.5 and 12.3 for different reactors, and the feed gas characteristic in the reformer of this study was about 11.1 as added in Figure 7 for comparison. It was assumed here that the $\frac{H_2 + CO}{H_2O + CO_2}$ molar ratio for the top gas of reactor is about 1.9 and it has a $H_2$/CO ratio of about 1.6, which is close to the other industrial modules where this ratio is between 1.5 and 2. It was found that changing this ratio does not affect much the later calculations and so these characteristics for the DRI process gas are hereafter considered.

Regarding the conversion of $Fe_2O_3$ to Fe by $H_2$ ($Fe_2O_3 + 3H_2 = 2Fe + 3H_2O$) and CO ($Fe_2O_3 + 3CO = 2Fe + 3CO_2$), the mass of metallic iron of DRI produced from hematite can be calculated as

$$m_{Fe}^{DRI} = \frac{2}{3} n_{RO}^{Fe} M_{Fe} \tag{28}$$

Similarly, the mass of $Fe^{2+}$ iron (FeO) in DRI produced from hematite can be calculated using

$$m_{FeO}^{DRI} = 2 n_{RO}^{FeO} M_{FeO} \tag{29}$$

where $n_{RO}^{Fe}$ and $n_{RO}^{FeO}$ are the number of moles (in kmol) of the reductant gases ($H_2$ + CO) that react with hematite for Fe and FeO formation, respectively. These two parameters are in relation to each other as

$$n_{RO}^{Fe} + n_{RO}^{FeO} = n_{RO}^{t} \tag{30}$$

where $n_{RO}^{t}$ denotes the total amount of $H_2$ and CO (in kmol) consumed in the reactor for the reduction reactions, and it is depending on the compositions and the amounts of the feed gas and top gas

$$n_{RO}^{t} = (\%\, H_2 + \%\, CO)_{feed} \cdot n_{feed} - (\%\, H_2 + \%\, CO)_{top} n_{top} \tag{31}$$

where $n_{feed}$ and $n_{top}$ denote the number of moles of feed gas and top gas (in kmol), respectively. These two parameters are almost the same as the same number of moles of $H_2O$ and $CO_2$ that are produced due to the consumption of $H_2$ and CO in the reactor. Regarding the definition of the metallization degree (MD), $m_{Fe}^{DRI}$ and $m_{FeO}^{DRI}$ are in relation with each other as

$$m_{Fe}^{DRI}\left(\frac{100 - MD}{100}\right) = m_{FeO}^{DRI}\left(\frac{MD \cdot M_{Fe}}{100 M_{FeO}}\right) \tag{32}$$

Hence, eqs 28−32 can be used to determine the masses of $m_{Fe}^{DRI}$ and $m_{FeO}^{DRI}$ as they are the only two unknowns for a given MD value. Furthermore, the mass of DRI produced by the utilized gas in the reactor is obtained as

$$m_{DRI} = \frac{m_{Fe}^{DRI} + m_{FeO}^{DRI}}{100 - m_{gangue}^{DRI}} \times 100 \tag{33}$$

where $m_{gangue}^{DRI}$ denotes the mass of gangue in the DRI, which is dependent on the properties of the utilized ore/agglomerate. For instance, the conversion of the feed gas to the top gas shown in Figure 7 is accompanied by the production of 1230 kg of DRI with a MD of 94.1%. The burden temperature in the ferromanganese reactor is higher than that in the DRI reactor, and the total CO + $H_2$ is higher. Therefore, in this study, a


https://doi.org/10.1021/acssuschemeng.0c08462
ACS Sustainable Chem. Eng. 2021, 9, 5010−5026

complete reduction of $Fe_2O_3$ in the burden of FeMn reactor was considered, while in the DRI reactor, an acceptable MD was considered. In principle, a higher MD in the DRI reactor is possible to obtain; however, in practice, the production rate is decreased. Considering the typical iron ore pellet composition given in Table 2, approximately 1702 kg iron ore pellet is reduced to produce this amount of DRI with the corresponding given composition as shown in the table.

It was observed that about 1230 kg DRI is produced per one-ton HCFeMn, and this may give the reader a feeling that it is not feasible to produce a small quantity of DRI per unit mass of ferromanganese. It is worth noting that the natural gas-based DRI reactors are operated with small sizes such as the Gilmore module with about 26.4 t/h (230,000 t/year), medium sizes such as the Siderca module with a 100 t/h production rate,[40] and very large ones with above a million t/year such as Midrex mega modules. In small steelmaking companies, the installation of small DRI units is favorable, and feasible to combine with the FeMn reactor. Alternatively, the installation of more than one FeMn reactor makes it possible to enlarge the size of the adjacent single DRI reactor to utilize the gases from several ferromanganese reactors. Currently, there are ferromanganese producers that have two or three SAF modules in a plant, and hence installing several ferromanganese reactors in a plant and combining with a large DRI module is feasible.

*3.3.2. Energy Balance for the DRI Reactor.* The main chemical reactions in the DRI reactor are endothermic, reactions 19 and 21−23, and they use a portion of the hot feed gas enthalpy. Obviously, small heat is released due to the reduction of Mn oxides to MnO, and most likely the water gas shift reaction will release more heat. On the other hand, a large portion of the enthalpy of the hot reducing feed gas is consumed for heating up the materials in the burden. Assuming the charge of cold iron ore pellet (room temperature) with the properties given in Table 2 to produce DRI with 900 °C temperature (in the upper part of the reactor), the reactor does not need any external heat supply as shown in Figure 8 for the case of feed gas

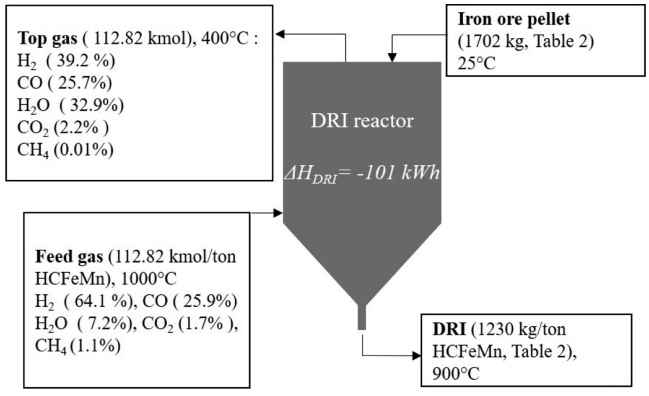


**Figure 8.** Overall mass balance and the characteristics of the input and the output of the DRI reactor.

and top gas temperatures of 1000 and 400 °C, respectively. Obviously, the negative enthalpy of about—101 kW h/t HCFeMn is enough to compensate the heat losses from the body of the DRI reactor. Hence, the DRI reactor does not need any external heat supply.

**3.4. Integrated Duplex Process and Energy Recovery.** As many commercial processes being developed today, the proposed duplex process needs to have energy recovery units to be run more economical and sustainable. Figure 9 shows the integrated process with materials flow and their temperatures (for the considered Mn ore in this study) with a few viable suggested energy recovery units by the author. As the top gas of the DRI reactor contains significant $H_2$ and CO species around 65%, and it has 400 °C, it has an enthalpy of about 3286 kW h/t HCFeMn. Therefore, it is crucially important to recover a part of this energy via power generation. It is worth mentioning that the energy recovery from the DRI process gas is common in the steel industry. Approximately 45% of this gas can be used in the gas reformer burners to supply the required heat for the reformer tubes and the corresponding endothermic reactions (about 1608 kW h/t HCFeMn), and the remained 55% can be used in an energy recovery unit to produce electricity and then add it to the FeMn reactor as shown in Figure 9. In addition, the reformer hot off-gas with around 1050 °C can be used in recuperators to heat up cold methane and air for the process to 500 and 400 °C, respectively. These temperatures are typical temperature chosen here by the author to extract typical numbers. As illustrated in Figure 9, the temperature of the reformer off-gas is decreased from 1050 °C heat exchangers to about 650 °C upon heat exchange with methane and air.

The remained DRI process gas (55%) is considered here to be used in a turbine to convert the thermal and chemical energy into electricity via combustion with air. This portion of gas has an enthalpy of 1807 kW h/t HCFeMn at 400 °C and its temperature can increase to about 2000 °C in combustion (with an enthalpy of about 1902 kW h/t HCFeMn), considering completed conversions of the $H_2$ and CO to $H_2O$ and $CO_2$. Like the scrubber of the FeMn reactor, the top gas temperature in the cleaning step is decreased (it was assumed to be in the range of 350−400 °C), however, it does not affect significantly the total enthalpy of the process gas. In turbine operation, the temperature can be controlled by controlling the air and turbine operation conditions. The current commercial gas or steam turbines can recover 40−65% of energy, depending on the utilized technology.[45] Assuming around 45% energy recovery by a modern energy recovery unit, about 856 kW h/t HCFeMn electric energy can be recovered for using in the FeMn reactor. Regarding the above calculated required electric energy for the FeMn reactor to be 1824 kW h/t HCFeMn, the supply of about 968.5 kW h/t HCFeMn is needed. This theoretical energy consumption is much lower than the SAF process, which is theoretically 241311 and 2193[9] kW h/t HCFeMn, excluding the raw material effect here. In average, SAF in industrial operation needs 2200−3200 kW h/t HCFeMn electricity.[46] It is worth noting that it is possible to recover more energy from the off-gases, and this energy recovery can be for different purposes such as warm water supply for houses, heating football fields, greenhouses, fish farms, and so forth as has been done in the Norwegian ferroalloy industry.[47]

**3.5. Process Sustainability.** To evaluate the sustainability of the presented duplex process, the electric energy consumption and $CO_2$ emission from the process are compared with available industrial numbers for the SAF process.

*3.5.1. Electric Energy Consumption.* The electric energy consumption in the duplex process is mostly related to the FeMn reactor and it is negligible for the DRI reactor as observed above. Hence, the comparison of the electric energy consumption is done here in comparison with the SAF for HCFeMn production. As described in Section 3.1, around 1824 kW h electric energy per ton HCFeMn is required for the stand-alone HC−FeMn reactor, if the utilized methane is preheated to 500 °C. This is


https://doi.org/10.1021/acssuschemeng.0c08462
ACS Sustainable Chem. Eng. 2021, 9, 5010−5026

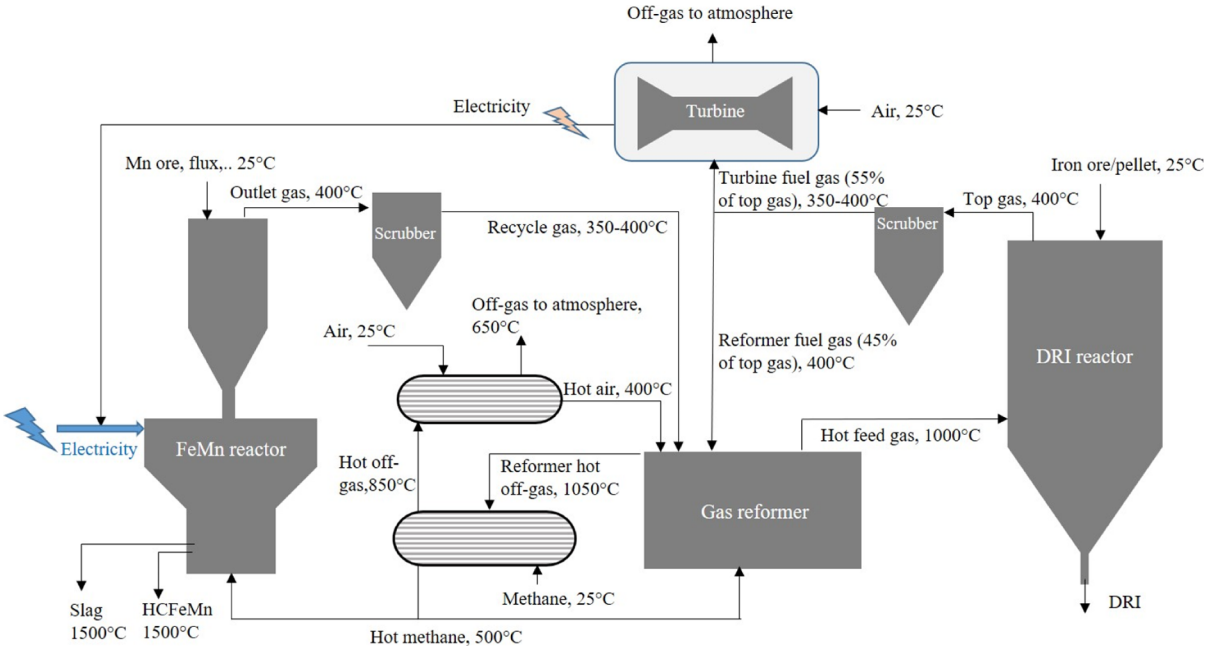


**Figure 9.** Integrated duplex FeMn-DRI process with energy recovery units.

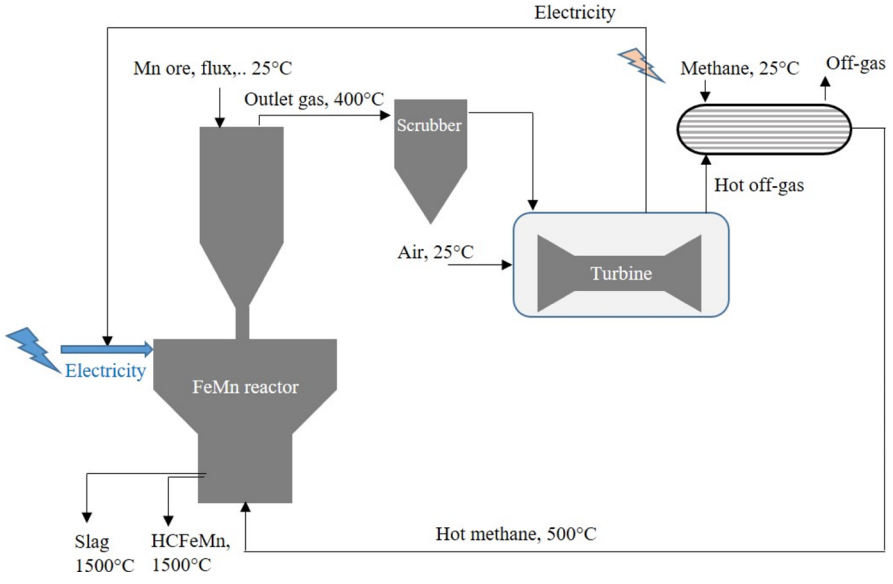


**Figure 10.** Schematic of the stand-alone FeMn reactor with an energy recovery unit.

obviously the theoretical value for the case that the FeMn process gas is not further used for DRI production. However, for the case of a stand-alone HCFeMn reactor with an energy recovery unit as illustrated in Figure 10, around 1063 kW h/t FeMn is recovered considering 45% efficiency for the turbine. Hence, the net required electric energy is about 867.2 kW h/t FeMn, which is significantly lower than that of a FeMn reactor with no energy recovery. On the other hand, it is lower than the integrated duplex process electric energy consumption of about 968.5 kW h/t HCFeMn (and 1.23 ton of DRI), which is rational as the whole FeMn reactor process gas has a slightly higher enthalpy (2107 kW h/t HCFeMn) than 55% of the top gas of the DRI reactor (1807 kW h/t HCFeMn). In order to show the effect of energy recovery, the required electric energy for the processes shown in Figures 9 and 10 was calculated as illustrated in Figure 11. Obviously, the electric energy consumption is increased using less-efficient turbines, and the energy consumption of the duplex process is slightly higher than that of the stand-alone FeMn reactor, for instance about 12% higher for 45% energy recovery. However, in the Duplex process, there is more added value due to DRI production and it may be more favorable. The stand-alone FeMn reactor with an energy recovery unit (Figure 10) can be an alternative to SAF for the ferroalloy industry.

Figure 12 shows the comparison of the above scenarios for the Duplex reactor in comparison with SAF. In order to calculate the energy consumption of the SAF, the same charge materials for the FeMn reactor above were considered with the same characteristics as those of the metal and slag products; however, instead of the methane solid, carbon was added into the charge. In order to maintain the same slag composition, it was a fair approximation to assume that the solid carbon charge is pure.



https://doi.org/10.1021/acssuschemeng.0c08462
ACS Sustainable Chem. Eng. 2021, 9, 5010−5026

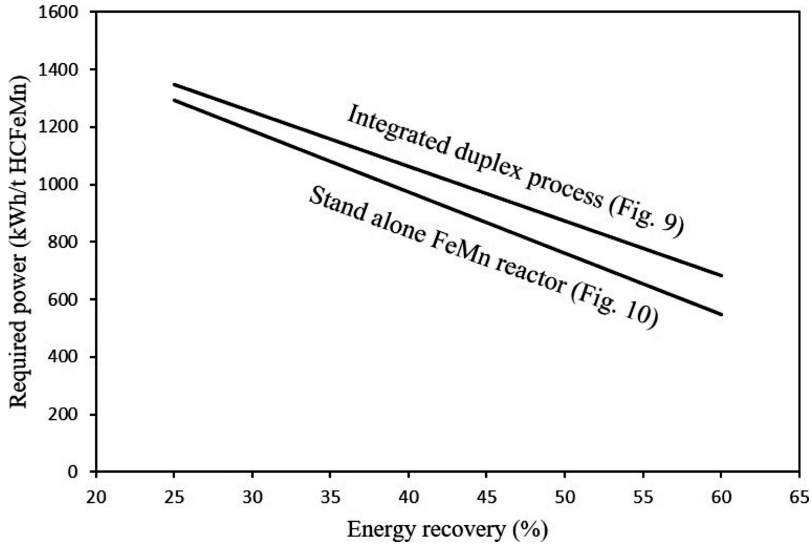


**Figure 11.** Relationship between the power required for the FeMn reactor and the efficiency of the energy recovery unit for two process scenarios.

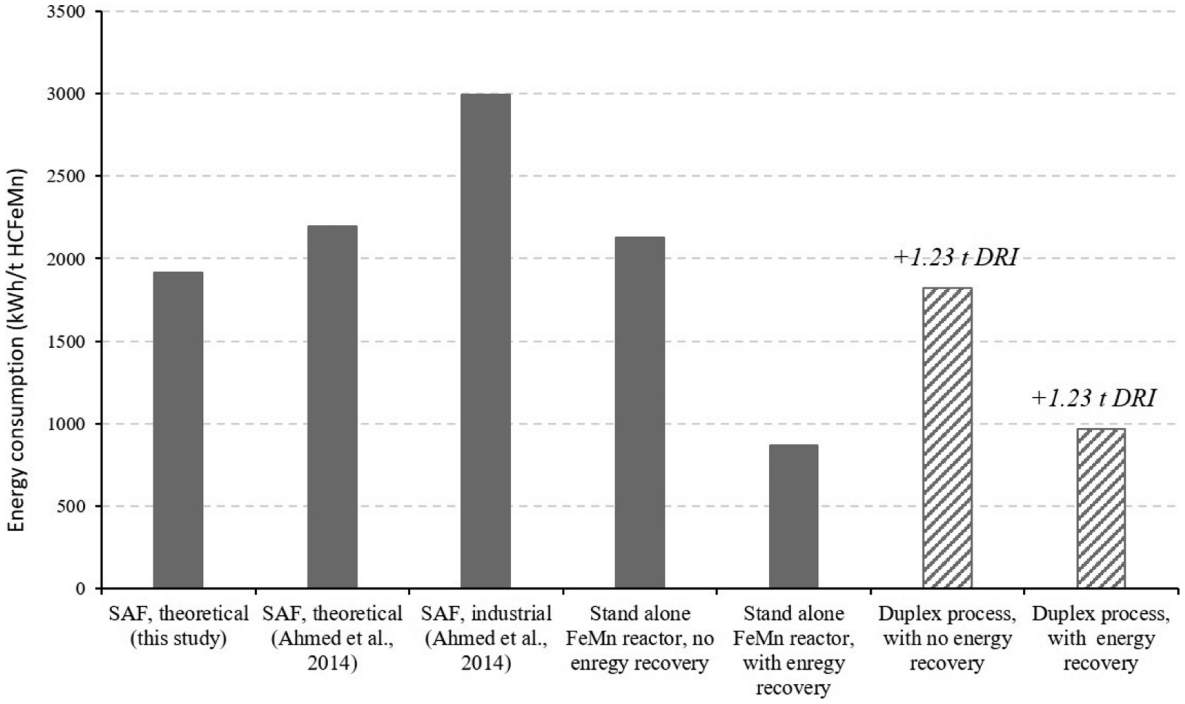


**Figure 12.** Comparison of energy consumption for HCFeMn (and DRI) production for different processes.

The mass balance calculation for the SAF reactor for the case of Boudouard reaction involvement with about 23% C consumption[9] indicated a total carbon consumption of about 335 kg/t FeMn, and correspondingly about 1914 kW h/t FeMn electric energy consumption was calculated. This theoretical value is relatively close to the theoretical value of 2193 kW h/t FeMn reported by Ahmed et al.[9] for balancing the energy of a 21 MVA commercial HCFeMn furnace with a real energy consumption of 2993 kW h/t FeMn. These numbers for SAF are for the units excluding energy recovery in the form of electricity. It is worth noting that Ahmed et al. have had different charge materials and a larger slag volume of 690 kg/t FeMn with about 19% MnO. They also calculated that 361 kW h/t FeMn is dedicated to the Boudouard reaction, and this energy corresponds to about 91 kg/t FeMn of carbon loss via this reaction. Regarding their total coke consumption and its carbon content, the Boudouard reaction consumes about 23% of the SAF carbon charge, which agrees with the literature. It is worth noting that a significant amount of alkalis, potassium, is cycled in the SAF and it acts as a catalyst for the Boudouard reaction and, therefore, this reaction proceeds well.[8,48] In short, the energy consumption of the FeMn reactor is slightly lower than that of the SAF; however, it is significantly lower via combining with an energy recovery. Obviously, the duplex process offers a better situation regarding the DRI production, accompanied by lower energy consumption per unit mass of all the metallic products.

Currently, no electric energy recovery from the off-gas of SAF is commercially done (author could not find) for HCFeMn production, while it is done in the other industries such as ferrosilicon and ferrochromium processes. Considering the


https://doi.org/10.1021/acssuschemeng.0c08462
ACS Sustainable Chem. Eng. 2021, 9, 5010−5026

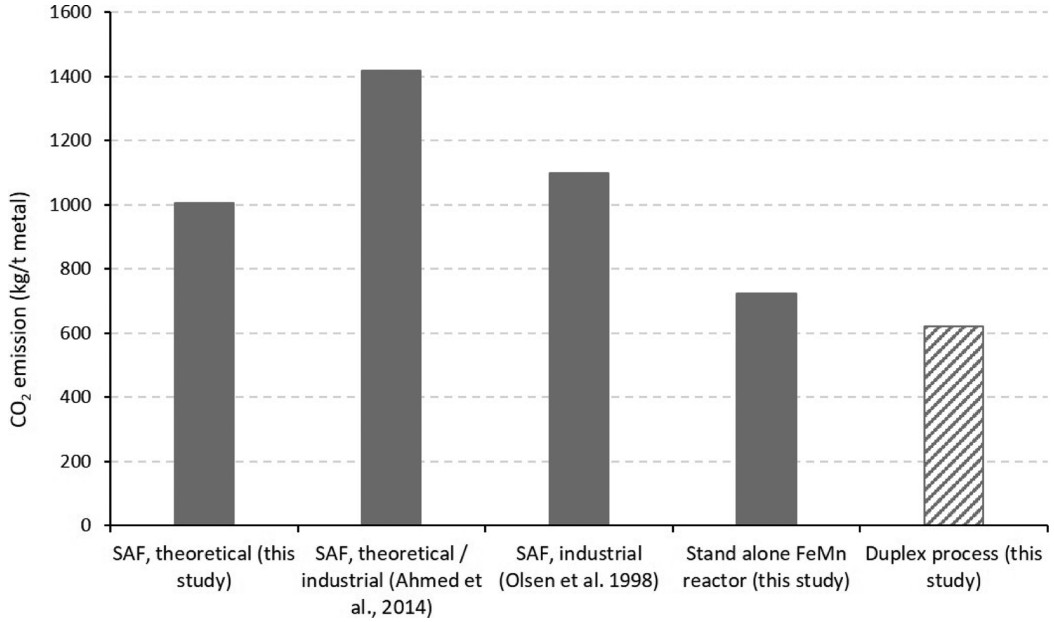


**Figure 13.** Comparison of $CO_2$ emission for HCFeMn (and DRI) production for different processes.

charge materials for the FeMn reactor for a SAF, about 28 kmol gas with a composition of 35% CO, 47% $CO_2$, 18% $H_2O$ was calculated at the outlet with a temperature of 200 °C. Electric energy recovery from this gas in a turbine with 45% recovery, as the above calculations for the FeMn reactor, returns about 780 kW h/t HCFeMn as calculated, which is about 70% of that for the stand-alone FeMn reactor. Hence, the SAF energy consumption is 1140 kW h/t HCFeMn. It is worth noting that for the calculations, the output temperature of combustion for the FeMn reactor gas was obtained to be about 2000 °C, while for the SAF, it was about 1400 °C, and in principle it means that it is possible to recover even more energy for the FeMn reactor case. On the other hand, the quantity and quality of the hot process gas of the FeMn reactor is much higher than that of the SAF, making it more favorable to invest on energy recovery units than the current SAF process.

*3.5.2. $CO_2$ Emission.* The presented duplex process is a low $CO_2$ emission process in comparison with the current SAF process for HCFeMn production. Figure 13 illustrates the calculated $CO_2$ emissions for SAF, a stand-alone FeMn reactor, and the duplex process with regard to the charge materials characteristics of this study. The calculated $CO_2$ generation for the SAF scenario is slightly less than the average $CO_2$ emission from the Norwegian plants, which is 1040−1150 kg/t HCFeMn.[49] The difference with the industrial analysis reported by Ahmed et al. is mainly due to the differences in the compositions of the raw materials. It is worth mentioning that 1100−1800 kg $CO_2$/t HCFeMn is produced in SAF.[46] Figure 12 indicates that for a given Mn ore/agglomerate (this study), a stand-alone FeMn reactor generates 28% less $CO_2$ than SAF, and the duplex process is the most sustainable approach with about 40% lower $CO_2$ emission than SAF.

**3.6. Future Technology Development.** In this study, a future cleaner technology than SAF for HCFeMn production was presented and there will be of course challenges to commercialize it, mainly due to the lack of knowledge in the ferromanganese industry about DRI production, or in iron and steel industries about ferroalloy production. Regarding the significant DRI production by the developed technologies, about 108 million tons DRI were produced in 2019 according to World Steel Association,[50] and hence the duplex process development requires the development of the FeMn reactor as it is different with the SAF and BF technologies. The presented scheme in Figure 1 is speculative, and there may be several approaches to design the reactor, which is above the scope of this work.

The presented duplex process is important regarding the circular economy. A silicomanganese (SiMn) furnace adjacent to the FeMn reactor to utilize the HCFeMn slag, which has still significant MnO for SiMn production is viable. This will be of importance regarding the utilization of low-grade Mn ores as many of such ores have quartz and $SiO_2$-containing minerals.[2,33] Moreover, there has been great interest in the development of high Mn-containing TRIP and TWIP steels in recent years.[51−53] Hence, the production of Mn ferroalloys together with DRI at high temperatures is viable to produce these TRIP and TWIP steels in a steelmaking plant. Such an integrated process to utilize the iron and Mn primary raw materials for making high Mn-containing steels is probably better to be carried out by the steelmakers as the molten steel alloy must be further treated to final steel products such as sheets, bars, and so forth, and the required expertise is more in the steel industry.

The duplex process is advantageous to be used in geographical locations with natural gas (resources or economically transported) and cheap (renewable) electricity are available. Additionally, it is better to have local or regional users/customers. Moreover, it needs knowledge and experience about both Mn-ferroalloy production and DRI production and related engineering disciplines, depending on the process parts to be installed. In addition, it is advantageous to be adjacent to a steelmaking plant rather than the ferromanganese and DRI plants to minimize the long transportation of the materials. The present work, however, is a basis for further research in the field and research on the FeMn reactor on lab and pilot scales.

## 4. CONCLUDING REMARKS

The mass and energy balances for a future duplex process to produce ferromanganese and DRI by natural gas were done


https://doi.org/10.1021/acssuschemeng.0c08462
ACS Sustainable Chem. Eng. 2021, 9, 5010−5026

considering the process thermochemistry. The main conclusions of this work are summarized as:

- The production of ferromanganese by natural gas is viable from the process chemistry point of view in a FeMn reactor, yielding a gaseous product with high amounts of CO and $H_2$ gases.
- The FeMn reactor gas outlet can be upgraded to a hot reducing gas for DRI production via methane reforming with it in a gas reformer.
- The duplex process yields more than one-ton DRI, that is, 1.23 t, per one-ton ferromanganese produced.
- Energy recovery from the gases in the Duplex process benefits the process significantly with around 50% per unit mass of metals produced.
- The duplex process shows 40% lower $CO_2$ emission compared with the current commercial process per unit mass of the metal products.
- It was found that a stand-alone FeMn reactor for the HCFeMn production with an energy recovery unit for the process gas is advantageous than the current SAF technology, with at least 30% less electric energy consumption.

## AUTHOR INFORMATION


### Corresponding Author

**Jafar Safarian** − *Norwegian University of Science and Technology (NTNU), NO-7491 Trondheim, Norway;* orcid.org/0000-0003-3584-8581; Email: jafar.safarian@ntnu.no

Complete contact information is available at: https://pubs.acs.org/10.1021/acssuschemeng.0c08462


### Notes

The author declares no competing financial interest.

## REFERENCES


(1) Olsen, S. E.; Tangstad, M.; Lindstad, T. *Production of Manganese Ferroalloys*; Tapir Academic Press: Trondheim, Norway, 2007.

(2) Cheraghi, A.; Yoozbashizadeh, H.; Ringdalen, E.; Safarian, J. Kinetics and Mechanism of Low-Grade Manganese Ore Reduction by Natural Gas. *Metall. Mater. Trans. B* **2019**, *50*, 1566−1580.

(3) Cheraghi, A.; Yoozbashizadeh, H.; Safarian, J. Gaseous Reduction of Manganese Ores: A Review and Theoretical Insight. *Miner. Process. Extr. Metall. Rev.* **2020**, *41*, 198−215.

(4) El-Gawad, H. H. A.; Ahmed, M. M.; El-Hussiny, N. A.; Shalabi, M. E. H. Reduction of Low Grade Egyptian Manganese Ore via Hydrogen at 800°C - 950°C. *OALib* **2014**, *01*, 1−11.

(5) Yastreboff, M.; Ostrovski, O.; Ganguly, S. Effect of Gas Composition on the Carbothermic Reduction of Manganese Oxide. *ISIJ Int.* **2003**, *43*, 161−165.

(6) Ostrovski, O. The Use of Natural Gas for Reduction of Metal Oxides: Constraints and Prospects. In *Celebrating the Megascale: Proceedings of the Extraction and Processing Division, Symposium on Pyrometallurgy in Honor of David G. C. Robertson*; Mackeiv, E. J., Jones, R. T., Brooks, G. A., Eds.; Springer: San Diego, California, USA, 2014; pp 529−536.

(7) Alizadeh, R.; Jamshidi, E.; Zhang, G. Transformation of methane to synthesis gas over metal oxides without using catalyst. *J. Nat. Gas Chem.* **2009**, *18*, 124−130.

(8) Lindstad, T.; Syvertsen, M.; Ishak, R. J.; Arntzen, H. B.; Grontvedt, P. O. The Influence of Alkalis on the Boudouard Reaction. *INFACON X*; Document Transformation Technologies: Cape Town, South Africa, 2004; pp 261−271.

(9) Ahmed, A.; Halfa, H.; El-Fawakhry, M. K.; El-Faramawy, H.; Eissa, M. Parameters Affecting Energy Consumption for Producing High Carbon Ferromanganese in a Closed Submerged Arc Furnace. *J. Iron Steel Res. Int.* **2014**, *21*, 666−672.

(10) Tanabe, I. Preheating of ore for a ferromanganese furnace—A recent trend in Japan. *Jom* **2017**, *20*, 81−87.

(11) Tangstad, M.; Ichihara, K.; Ringdalen, E. Pretreatment unit in ferromanganese production. *INFACON XIV*; Kiev: Ukraine, 2015; pp 99−106.

(12) Safarian, J.; Tranell, G.; Kolbeinsen, L.; Tangstad, M.; Gaal, S.; Kaczorowski, J. Reduction Kinetics of MnO from High-Carbon Ferromanganese Slags by Carbonaceous Materials in Ar and CO Atmospheres. *Metall. Mater. Trans. B* **2008**, *39*, 702−712.

(13) Guo, S.; Jiang, G. C.; Xu, J. L.; Xu, K. D. Kinetics of reduction of MnO in molten slag with carbon undersaturated liquid iron. *J. Iron Steel Res. Int.* **2000**, *7*, 1−5.

(14) Daines, W. L.; Pehlke, R. D. Kinetics of manganese oxide reduction from basic slags by silicon and carbon dissolved in liquid iron. *Metall. Trans.* **1971**, *2*, 1203−1211.

(15) Tarby, S. K.; Philbrook, W. O. The rate and mechanism of the reduction of FeO and MnO from silicate and aluminate slags by carbon−saturated iron. *Trans. Metall. Soc. AIME* **1967**, *239*, 1005−1017.

(16) Pomfret, R. J.; Grieveson, P. Kinetics of fast initial stage of reduction of MnO from silicate slags by carbon in molten iron. *Ironmaking Steelmaking* **1978**, *5*, 191−197.

(17) Upadhya, K. The kinetics and mechanism(s) of manganese oxide reduction from liquid slag by carbon dissolved in iron. *Trans. Iron Steel Soc.* **1986**, *7*, 1−6.

(18) Safarian, J., Kolbeinsen, L., Grong, Ø. Kinetic Modelling of MnO Reduction from Slags by Dissolved Carbon in Liquid Iron. In *Sohn International Symposium Advanced Processing of Metals and Materials, Volume 1—Thermo and Physicochemical Principles: Non-Ferrous High-Temperature Processing*; Kongoli, R. G., Ed.: San Diego, California, 2006; pp 125−139.

(19) Abbas, H. F.; Wan Daud, W. M. A. Hydrogen production by methane decomposition: A review. *Int. J. Hydrogen Energy* **2010**, *35*, 1160−1190.

(20) Steinberg, M. The Carnol process for CO2 mitigation from power plants and the transportation sector. *Energy Convers. Manage.* **1996**, *37*, 843−848.

(21) Serban, M.; Lewis, M. A.; Marshall, C. L.; Doctor, R. D. Hydrogen Production by Direct Contact Pyrolysis of Natural Gas. *Energy Fuels* **2003**, *17*, 705−713.

(22) Plevan, M.; Geißler, T.; Abánades, A.; Mehravaran, K.; Rathnam, R. K.; Rubbia, C.; Salmieri, D.; Stoppel, L.; Stückrad, S.; Wetzel, T. Thermal cracking of methane in a liquid metal bubble column reactor: Experiments and kinetic analysis. *Int. J. Hydrogen Energy* **2015**, *40*, 8020−8033.

(23) Geißler, T.; Abánades, A.; Heinzel, A.; Mehravaran, K.; Müller, G.; Rathnam, R. K.; Rubbia, C.; Salmieri, D.; Stoppel, L.; Stückrad, S.; Weisenburger, A.; Wenninger, H.; Wetzel, T. Hydrogen production via methane pyrolysis in a liquid metal bubble column reactor with a packed bed. *Chem. Eng. J.* **2016**, *299*, 192−200.

(24) Upham, D. C.; Agarwal, V.; Khechfe, A.; Snodgrass, Z. R.; Gordon, M. J.; Metiu, H.; McFarland, E. W. Catalytic molten metals for the direct conversion of methane to hydrogen and separable carbon. *Science* **2017**, *358*, 917.

(25) Safarian, J.; Kolbeinsen, L. Kinetic of carbothermic reduction of MnO from high-carbon ferromanganese slag by graphite materials. *ISIJ Int.* **2008**, *48*, 395−404.

(26) Safarian, J., Kinetics and mechanisms of reduction of MnO-containing silicate slags by selected forms of carbonaceous materials. PhD Thesis, NTNU: Trondheim, Norway, 2007; p 250.

(27) Rodat, S.; Abanades, S.; Coulié, J.; Flamant, G. Kinetic modelling of methane decomposition in a tubular solar reactor. *Chem. Eng. J.* **2009**, *146*, 120−127.

(28) Fincke, J. R.; Anderson, R. P.; Hyde, T. A.; Detering, B. A. Plasma Pyrolysis of Methane to Hydrogen and Carbon Black. *Ind. Eng. Chem. Res.* **2002**, *41*, 1425−1435.
(29) ASTM-A99-82. *ASTM A99-82(2000), Standard Specification for Ferromanganese*; ASTM International: West Conshohocken, PA, USA, 2000.
(30) Tangstad, M. The High-Carbon Ferromanganese Process—Coke Bed Relations. *Materials Science and Engineering*; Norwegian Institute of Technology (NTH): Trondheim, Norway, 1996.
(31) Olsø, V. T. M.; Olsen, S. E. Reduction Kinetics of MnO-Saturated Slags. *INFACON VIII*, 1998; pp 279−283.
(32) Sorensen, B.; Gaal, S.; Ringdalen, E.; Tangstad, M.; Kononov, R.; Ostrovski, O. Phase compositions of manganese ores and their change in the process of calcination. *Int. J. Miner. Process.* **2010**, *94*, 101−110.
(33) Cheraghi, A.; Becker, H.; Eftekhari, H.; Yoozbashizadeh, H.; Safarian, J. Characterization and calcination behavior of a low-grade manganese ore. *Mater. Today Commun.* **2020**, *25*, 101382.
(34) Ostrovski, O.; Olsen, S. E.; Tangstad, M.; Yastreboff, M. Kinetic Modelling of MnO Reduction from Manganese Ore. *Can. Metall. Q.* **2002**, *41*, 309−318.
(35) Huang, W. An assessment of the Fe-Mn system. *Calphad* **1989**, *13*, 243−252.
(36) Hoel, E. G. *Structures and Phase Relations in Silicomanganese Alloys*; Department of Metallurgy, Norwegian University of Science and Technology: Trondheim, 1998; X, 170, [186] s. ill.
(37) Midrex Technologies Inc. *MIDREX NG, Optimizing DRI Production Using Natural Gas*, 2014.
(38) Feinman, J.; MacRae, D. R. Direct Reduced Iron. *Technology and Economics of Production and Use*; Iron and Steel Society: Warrendale, PA (United States), 1999.
(39) Szekely, J., Evans, J. W., Sohn, H. Y. *Gas−Solid Reactions*; Elsevier Science, 1976.
(40) Parisi, D. R.; Laborde, M. A. Modeling of counter current moving bed gas-solid reactor used in direct reduction of iron ore. *Chem. Eng. J.* **2004**, *104*, 35−43.
(41) Valipour, M. S.; Saboohi, Y. Numerical investigation of nonisothermal reduction of hematite using Syngas: The shaft scale study. *Modell. Simul. Mater. Sci. Eng.* **2007**, *15*, 487−507.
(42) Shams, A.; Moazeni, F. Modeling and Simulation of the MIDREX Shaft Furnace: Reduction, Transition and Cooling Zones. *JOM* **2015**, *67*, 2681−2689.
(43) Zare Ghadi, A.; Valipour, M. S.; Biglari, M. CFD simulation of two-phase gas-particle flow in the Midrex shaft furnace: The effect of twin gas injection system on the performance of the reactor. *Int. J. Hydrogen Energy* **2017**, *42*, 103−118.
(44) Béchara, R.; Hamadeh, H.; Mirgaux, O.; Patisson, F. Optimization of the Iron Ore Direct Reduction Process through Multiscale Process Modeling. *Materials* **2018**, *11*, 1094.
(45) Benini, E. Advances in Gas Turbine Technology. *Future Aero Engine Designs: An Evolving Vision*, 1st ed.; InTech: Rijeka, Croatia, 2011.
(46) Cusano, G. G.; Farrell, F.; Remus, R.; Roudier, S.; Sancho, L. D. Best Available Techniques (BAT) Reference Document for the Non-Ferrous Metals Industries. *Industrial Emissions Directive 2010/75/EU, Integrated Pollution Prevention and Control*; Publications Office of the European Union, 2017.
(47) Kamfjord, N. E.; Myrhaug, E. H.; Tveit, H.; Wittgens, B. Energy Balance of a 45 MW/Ferro-Silicon Submerged Arc Furnace. *INFACON XII*; Finland: Helsinki, 2010; pp 729−738.
(48) Kaczorowski, J.; Lindstad, T.; Syvertsen, M. The Influence of Potassium on the Boudouard Reaction in Manganese Production. *ISIJ Int.* **2007**, *47*, 1599−1604.
(49) Olsen, S. E., Monsen, B. E.; Lindstad, T. $CO_2$-Emissions from the Production of Manganese and Chromium Alloys in Norway. In *56th Electric Furnace Conference Proceedings*; Stendera, J. W., Ed.; Iron and Steel Society: New Orleans, Louisiana, USA, 1998; pp 1−7.
(50) World-Steel-Association. *2020 World Steel in Figures*, 2020; p 19.
(51) Steinmetz, D. R.; Jäpel, T.; Wietbrock, B.; Eisenlohr, P.; Gutierrez-Urrutia, I.; Saeed−Akbari, A.; Hickel, T.; Roters, F.; Raabe, D. Revealing the strain-hardening behavior of twinning-induced plasticity steels: Theory, simulations, experiments. *Acta Mater.* **2013**, *61*, 494−510.
(52) Haldar, A.; Suwas, S.; Bhattacharjee, D. *Microstructure and Texture in Steels*; Springer, 2009.
(53) Safarian, J.; Kolbeinsen, L. Purity Requirements for Mn-Alloys for Producing High Manganese TRIP and TWIP Steels. *The Thirteenth International Ferroalloys Congress (INFACON XIII)*; Almaty: Kazakhstan, 2013; pp 175−183.


https://doi.org/10.1021/acssuschemeng.0c08462
*ACS Sustainable Chem. Eng.* 2021, 9, 5010−5026